Article

Cell Host & Microbe

SMAC Mimetics Induce Autophagy-Dependent Apoptosis of HIV-1-Infected Resting Memory CD4+ T Cells

Graphical Abstract

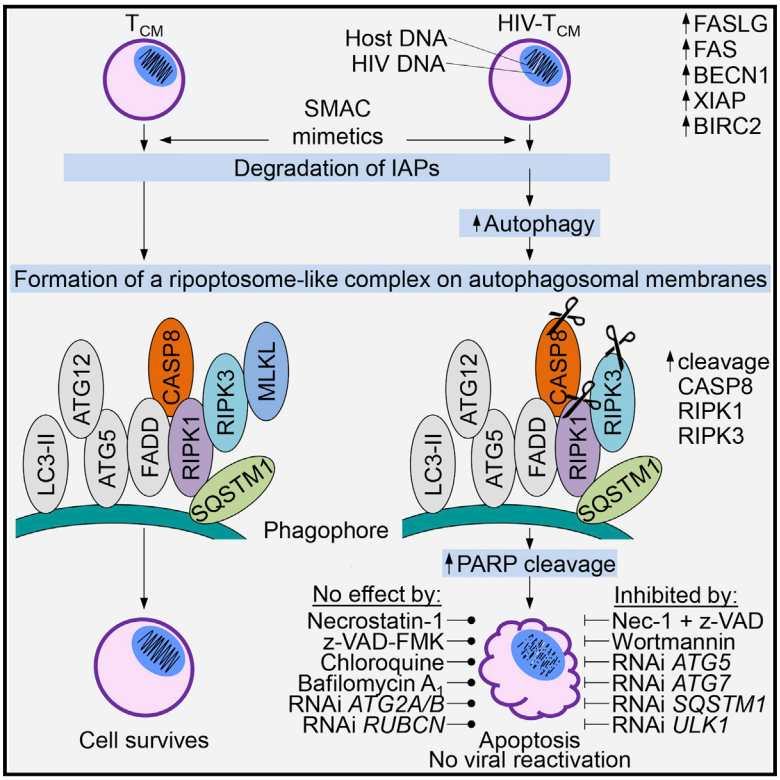

Highlights

- SMAC mimetics selectively induce apoptosis in HIV-infected resting memory CD4+ T cells
- SMAC mimetic-mediated apoptosis is dependent upon autophagy induction and factors
- SMAC mimetics exploit autophagy proteins to assemble a death-inducing signaling complex
- Inhibition of autophagy induction, but not degradation, abrogates SMAC mimetic efficacy

Authors

Grant R. Campbell, Rachel S. Bruckman, Yen-Lin Chu, Rodney N. Trout, Stephen A. Spector

Correspondence

saspector@ucsd.edu

In Brief

Ineffective eradication of HIV reservoirs impedes cure. Campbell et al. reveal that DIABLO/SMAC mimetics trigger apoptosis in HIV-infected resting memory CD4+ T cells, while having minimal effect on uninfected cells. This selective killing requires the induction of autophagy and formation of a ripoptosome-like cytosolic death-inducing signaling complex.

Campbell et al., 2018, Cell Host & Microbe *24*, 1–14
November 14, 2018
https://doi.org/10.1016/j.chom.2018.09.007

CellPress

Please cite this article in press as: Campbell et al., SMAC Mimetics Induce Autophagy-Dependent Apoptosis of HIV-1-Infected Resting Memory CD4+ T Cells, Cell Host & Microbe (2018), https://doi.org/10.1016/j.chom.2018.09.007

Cell Host & Microbe
Article

SMAC Mimetics Induce Autophagy-Dependent Apoptosis of HIV-1-Infected Resting Memory CD4+ T Cells

Grant R. Campbell,[1] Rachel S. Bruckman,[1,3] Yen-Lin Chu,[1,4] Rodney N. Trout,[1] and Stephen A. Spector[1,2,5,*]
[1]Division of Infectious Diseases, Department of Pediatrics, University of California San Diego, La Jolla, CA 92093, USA
[2]Rady Children's Hospital, San Diego, CA 92123, USA
[3]Present address: Chicago Medical School, Rosalind Franklin University of Medicine and Science, North Chicago, IL 60064, USA
[4]Present address: Epic Sciences, San Diego, CA 92121, USA
[5]Lead Contact
*Correspondence: saspector@ucsd.edu
https://doi.org/10.1016/j.chom.2018.09.007

SUMMARY

Long-lived resting memory CD4+ T cells (T_{CM}) are a major reservoir of latent HIV infection. We hypothesized that latent HIV-T_{CM} cells are maintained by aberrant expression of cell survival factors, including XIAP, BIRC2/cIAP1, and beclin-1. DIABLO/SMAC mimetics are therapeutic agents that compromise cell survival by hijacking host apoptotic machinery. We found that DIABLO/SMAC mimetics (birinapant, GDC-0152, and embelin) selectively kill HIV-T_{CM} without increasing virus production or targeting uninfected T_{CM}. Treatment of HIV-T_{CM} with DIABLO/SMAC mimetics promoted XIAP and BIRC2 degradation, which triggered autophagy and the formation of a cell death complex consisting of pro-apoptotic (FADD, RIPK1, RIPK3, and caspase 8) and autophagy (ATG5, ATG7, and SQSTM1) proteins. Genetic or pharmacological inhibition of autophagy induction, but not autophagy-mediated degradation, abrogated this interaction and subsequent cell death. Our findings identify a mechanism whereby DIABLO/SMAC mimetics exploit autophagy and apoptotic machinery to selectively induce killing of HIV-T_{CM} without viral reactivation while sparing uninfected cells.

INTRODUCTION

The major obstacle to eradicating human immunodeficiency type-1 (HIV) is the establishment of long-lived reservoirs of virus. Latently infected cells containing replication-competent proviral DNA may survive for months to years and undergo proliferative renewal. Although antiretroviral therapy (ART) effectively suppresses HIV replication, persistent residual low-level viremia maintains the latent pool (Hermankova et al., 2001; Ramratnam et al., 2000). The very low expression of viral proteins enables latently infected cells to evade detection and clearance by the immune system. Thus, lifelong ART is required for continued viral suppression.

Autophagy is a degradation pathway that occurs at basal levels in all cells whereby cytosolic double membrane-bound compartments termed autophagosomes engulf and sequester cytoplasmic constituents such as sub-cellular organelles and microbial pathogens. Fusion with a lysosome generates an autolysosome, which enzymatically degrades the engulfed components. Autophagy is upregulated in response to stress such as starvation, drug treatment, and infection, and although predominantly a cell survival mechanism, under certain cellular conditions it can promote cell death (Fitzwalter and Thorburn, 2015). For example, autophagy promotes Fas cell surface death receptor (FAS)-mediated apoptosis by selectively degrading protein tyrosine phosphatase non-receptor type 13 (PTPN13), a negative regulator of FAS signaling in type I cells (Gump et al., 2014). In contrast, autophagy can also protect against tumor necrosis factor (TNF) superfamily member 10-induced apoptosis by controlling the levels of the pro-apoptotic BCL2-binding component 3 (BBC3) (Thorburn et al., 2014).

During HIV infection, CD4+ T cells produce interleukin (IL) 2, upregulate FAS and other pro-apoptotic molecules, and change from an apoptosis-resistant state to a post-activation and apoptosis-prone state. However, the expression of apoptosis regulatory proteins such as BCL2 family members and the inhibitor of apoptosis proteins (IAP) govern the susceptibility of the cell to undergo FAS-mediated death. HIV alters the transcriptional profile of some cell types to produce more endogenous apoptosis regulatory proteins. For example, HIV Tat upregulates anti-apoptotic proteins including BCL2, CFLAR (caspase [CASP] 8 and Fas-associated via death domain [FADD]-like apoptosis regulator), X-linked inhibitor of apoptosis (XIAP), and baculoviral IAP repeat containing 2 (BIRC2, formerly known as cIAP1) (López-Huertas et al., 2013). Similarly, HIV Nef induces the phosphorylation and inactivation of pro-apoptotic BCL2-associated agonist of cell death (BAD) (Wolf et al., 2001).

Overexpression of IAPs can inhibit cell death through a number of mechanisms, including direct inhibition of caspases and ubiquitination of receptor-interacting protein kinase (RIPK) 1, a potent activator of multiple forms of programmed cell death. Ubiquitinated RIPK1 can downregulate FAS signaling through NFKB-dependent proinflammatory signaling. Therefore, RIPK1 is a key convergence point between pro-death, pro-survival, and proinflammatory signals. Upon activation of the intrinsic apoptosis pathway, mitochondria release both cytochrome *c*

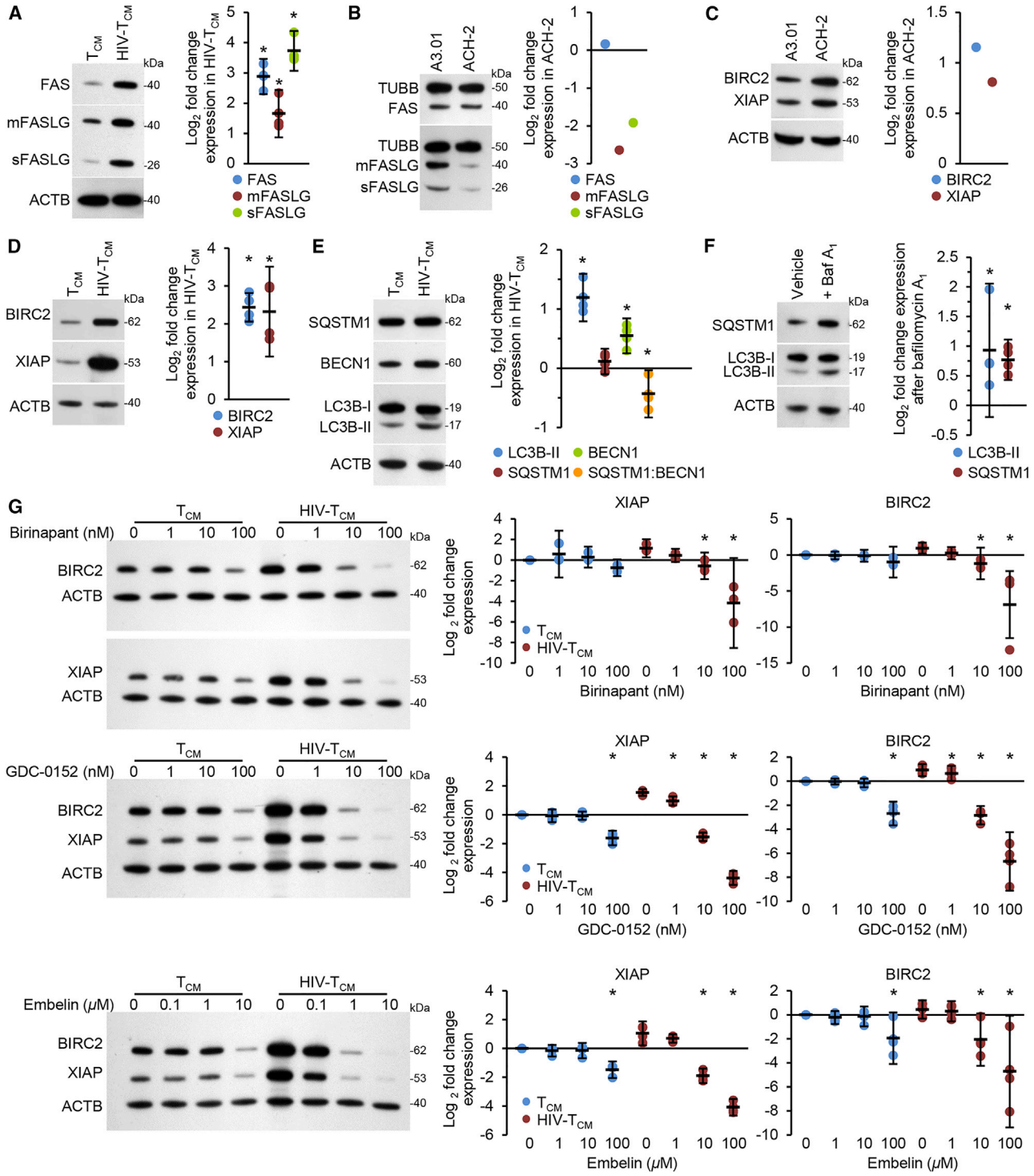

Figure 1. SMAC Mimetics Induce the Degradation of BIRC2 and XIAP in HIV-T_{CM}

(A) Left, representative western blots of FAS, membrane-bound FASLG (mFASLG), and soluble FASLG (sFASLG) in T_{CM} and HIV-T_{CM}. Right, densitometric analysis of blots. n = 4.

(B) Left, representative western blots of FAS, mFASLG and sFASLG in A3.01 and ACH-2. Experiment was performed in triplicate. Right, densitometric analysis of blots.

(C) Left, representative western blots of XIAP and BIRC2 in A3.01 and ACH-2. Experiment was performed in triplicate. Right, densitometric analysis of blots.

(D) Left, representative western blots of XIAP and BIRC2 in T_{CM} and HIV-T_{CM} using antibody to XIAP, BIRC2, and ACTB. Right, densitometric analysis of blots. n = 4.

(E) Left, representative western blots of LC3B isoforms, BECN1, and SQSTM1 in T_{CM} and HIV-T_{CM}. Right, densitometric analysis of blots. n = 4.

(legend continued on next page)

and diablo IAP-binding mitochondrial protein (DIABLO, formerly known as second mitochondria-derived activator of caspase [SMAC]). DIABLO is a pro-apoptotic protein that binds to and antagonizes IAP proteins. DIABLO directly competes with caspases for XIAP binding, liberating caspases for apoptosis. It can also stimulate the E3 ubiquitin ligase activity of BIRC2 and BIRC3 (formerly known as cIAP2), triggering their degradation via the proteasome. To circumvent the ability of IAP to turn pro-death into pro-survival signals, small-molecule DIABLO/SMAC peptidomimetics (SM) were developed that mimic the N-terminal four amino acid sequence of DIABLO required for IAP binding. The interaction of SM with XIAP leads to caspase activation (Gao et al., 2007), while the binding of SM to BIRC2 and BIRC3 enhances their E3 ligase activity, promoting their autoubiquitination and proteasomal degradation with subsequent cell death (Bertrand et al., 2008; Varfolomeev et al., 2007). A number of SM are in clinical trials as cancer therapeutics. IAP are relevant targets for therapeutic exploitation in HIV since they block programmed cell death, and both primary cells and cell lines latently infected with HIV display enhanced XIAP and BIRC2 expression (Berro et al., 2007; López-Huertas et al., 2013), which may play a role in the establishment of latency and cytopathogenesis (Wang et al., 2011). Moreover, BIRC2 and BIRC3 specifically mediate macrophage resistance to HIV Vpr-induced apoptosis (Busca et al., 2012), and alvocidib, a flavonoid alkaloid cyclin-dependent kinase 9 (CDK9) inhibitor, downregulates XIAP and significantly induces the latently infected ACH-2 cell line, but not the uninfected parental cell line, to undergo apoptosis (Berro et al., 2007). In this study, we examined the potential application of the SM embelin, GDC-0152, and birinapant to induce selective cell death in CD4+ T cells infected with HIV *in vitro* and *ex vivo*.

RESULTS

FAS, FASLG, XIAP, and BIRC2 Are Upregulated in HIV-Infected CD4+ T Cells

In HIV-infected individuals, CD4+ T cells overexpress Fas ligand (FasL or FASLG), are more susceptible to FASLG-induced apoptosis (Silvestris et al., 1996), and the rate of apoptosis correlates with surface levels of both FAS and FASLG (Silvestris et al., 1996). Therefore, we assessed the expression of FASLG and FAS in HIV-infected, resting central memory CD4+ T cells (HIV-T_{CM}) compared with resting, mock-infected central memory CD4+ T cells (T_{CM}). We observed enhanced expression of FAS as well as both membrane-bound and soluble FASLG in HIV-T_{CM} compared with T_{CM} (Figure 1A). Contrary to this, ACH-2 express similar levels of FAS as A3.01 while FASLG expression is downregulated (Figure 1B) (Pinti et al., 1999). FAS activation of apoptotic pathways in different cell types may be associated with differences in the extent of FAS aggregation or internalization, caspase cascade activation, and/or the levels of caspase inhibitors such as BIRC2 and XIAP. Therefore, we examined the expression of BIRC2 and XIAP as ACH-2 cells have increased expression of XIAP and BIRC2 (Figure 1C) (Berro et al., 2007); XIAP and BIRC2 (Figure 1D) were significantly upregulated in HIV-T_{CM} from all donors.

Upregulation of XIAP and BIRC2 leads to increased expression of beclin 1 (BECN1) through the activation of NFKB. Consistent with this, BECN1 expression was increased in HIV-T_{CM} (Figure 1E). Unlike other BH3-only proteins, the overexpression of BECN1 does not function as a pro-apoptotic signal but instead leads to increased autophagy (Lin et al., 2015). As HIV requires autophagy for replication (Campbell and Spector, 2013), we assessed the autophagic status of HIV-T_{CM}. During autophagy, an ubiquitin-like system that involves autophagy related (ATG) 7, ATG3, and the ATG12–ATG5 complex converts cytosolic microtubule-associated protein 1 light chain 3 beta (MAP1LC3B or LC3B)-I to LC3B-II. The ATG12–ATG5 complex then ligates LC3B-II to the nascent autophagosome membrane. The polyubiquitin-binding protein sequestosome 1 (SQSTM1, p62) and SQSTM1-bound polyubiquitinated proteins are also incorporated into completed autophagosomes. These autophagosomes then fuse with lysosomes, resulting in the degradation of the engulfed components as well as the LC3B-II and SQSTM1 associated with the inner membrane. Thus, the quantification of SQSTM1 and the conversion of LC3B-I to LC3B-II and its turnover are indicators of autophagy induction and flux (Klionsky et al., 2016). Compared with T_{CM} we observed a significant increase in LC3B-II and no change in SQSTM1 expression in HIV-T_{CM}. The latter resulted in a decrease in the SQSTM1:BECN1 protein ratio (Kara et al., 2013) and suggested augmented autophagy induction but an arrest in autophagic degradation. To confirm this, we used bafilomycin A_1, an inhibitor of V-ATPase and thus autophago-lysosome fusion and lysosomal degradation (Klionsky et al., 2016). LC3B-II and SQSTM1 were both increased, suggesting increased autophagy induction (Figure 1F).

SMAC Mimetics Trigger Rapid Degradation of BIRC2 and XIAP

As both BIRC2 and XIAP are upregulated in HIV-T_{CM}, we examined the effect of the SM GDC-0152, embelin, and birinapant on BIRC2 and XIAP content in HIV-T_{CM} and T_{CM}. All three SM induced a dose-dependent rapid degradation of both XIAP and BIRC2 that became significant at one-tenth the concentration in HIV-T_{CM} compared with T_{CM} (Figure 1G). Although SM induce the proteasomal degradation of IAP, we examined whether they also stimulate autophagy in HIV-T_{CM}. In T_{CM}, SM induced an increase in BECN1 expression and LC3B conversion but no significant SQSTM1 degradation (Figure 2A). In contrast, we observed significant SM-induced BECN1 expression, LC3B-II conversion, SQSTM1 degradation, and a decrease in the SQSTM1:BECN1 ratio in HIV-T_{CM} at 1 nM birinapant, 10 μM embelin, and 10 nM GDC-0152, suggesting induced autophagy (Figure 2A). To establish further the induction of autophagy in

(F) HIV-T_{CM} were treated for 4 hr with 100 nM bafilomycin A_1. Left, representative western blots of LC3B isoforms and SQSTM1. Right, densitometric analysis of blots. n = 4.

(G) T_{CM} and HIV-T_{CM} were treated for 24 hr with increasing concentrations of birinapant, GDC-0152, or embelin. Left, representative western blots of XIAP and BIRC2. Right, densitometric analysis of blots. n = 4.

For (A), (D), (E), (F), and (G), each symbol represents one donor. Error bars show mean ± 95% confidence interval. *p < 0.05 determined by Student's t test.

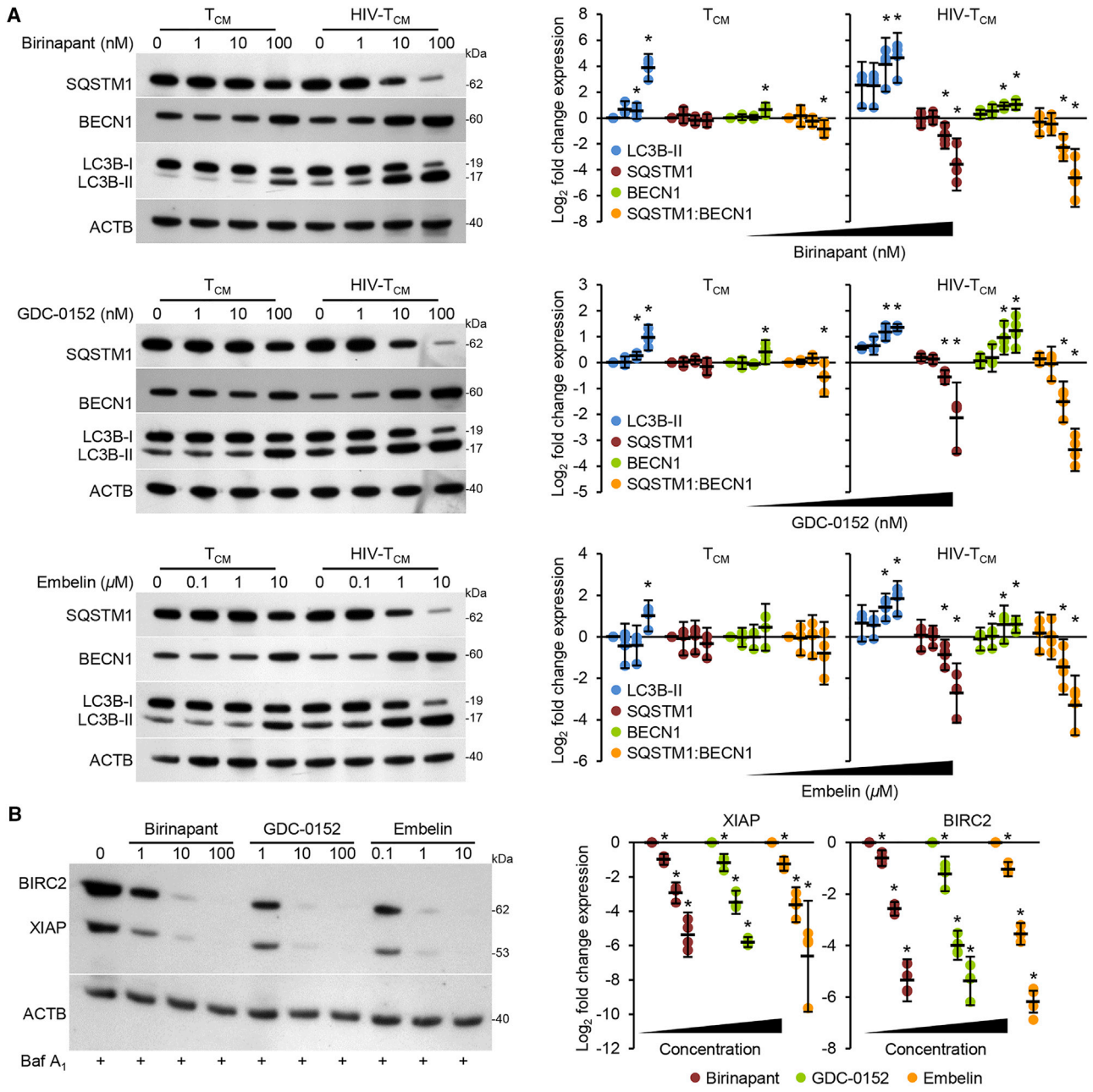

Figure 2. SMAC Mimetics Induce Autophagy in HIV-T_{CM}

(A) T_{CM} and HIV-T_{CM} were treated for 24 hr with SM. Left, representative western blots of LC3B isoforms, BECN1, and SQSTM1. Right, densitometric analysis of blots. n = 4.

(B) HIV-T_{CM} were pretreated with bafilomycin A_1 before incubation with SM for 24 hr. Left, representative western blots. Right, densitometric analysis of blots. n = 4. Each symbol represents one donor. Error bars show mean ± 95% confidence interval. *p < 0.05 determined by Student's t test.

SM-treated HIV-T_{CM}, and not simply the activation of *MAP1LC3B* and *SQSTM1* transcription, we used bafilomycin A_1. Blots of cell lysates confirmed autophagic flux in HIV-T_{CM}, with increased LC3B-II and SQSTM1 accumulation in bafilomycin A_1-treated cells relative to vehicle controls (Figure S2A). Importantly, as SQSTM1 is also a substrate for CASP6 and CASP8 (as well as calpain 1) (Norman et al., 2010), we still observed significant SQSTM1 degradation in the presence of a pan-caspase inhibitor (Figure S2B), and inhibition of the degradative steps of autophagy with bafilomycin A_1 had no effect on SM-induced XIAP or BIRC2 degradation in HIV-T_{CM} (Figure 2B).

SMAC Mimetics Selectively Kill Resting, HIV-Infected CD4+ T Cells

SM can stimulate cell death alone or in combination with pro-apoptotic TNF-family ligands (Fulda, 2015). Since both FASLG

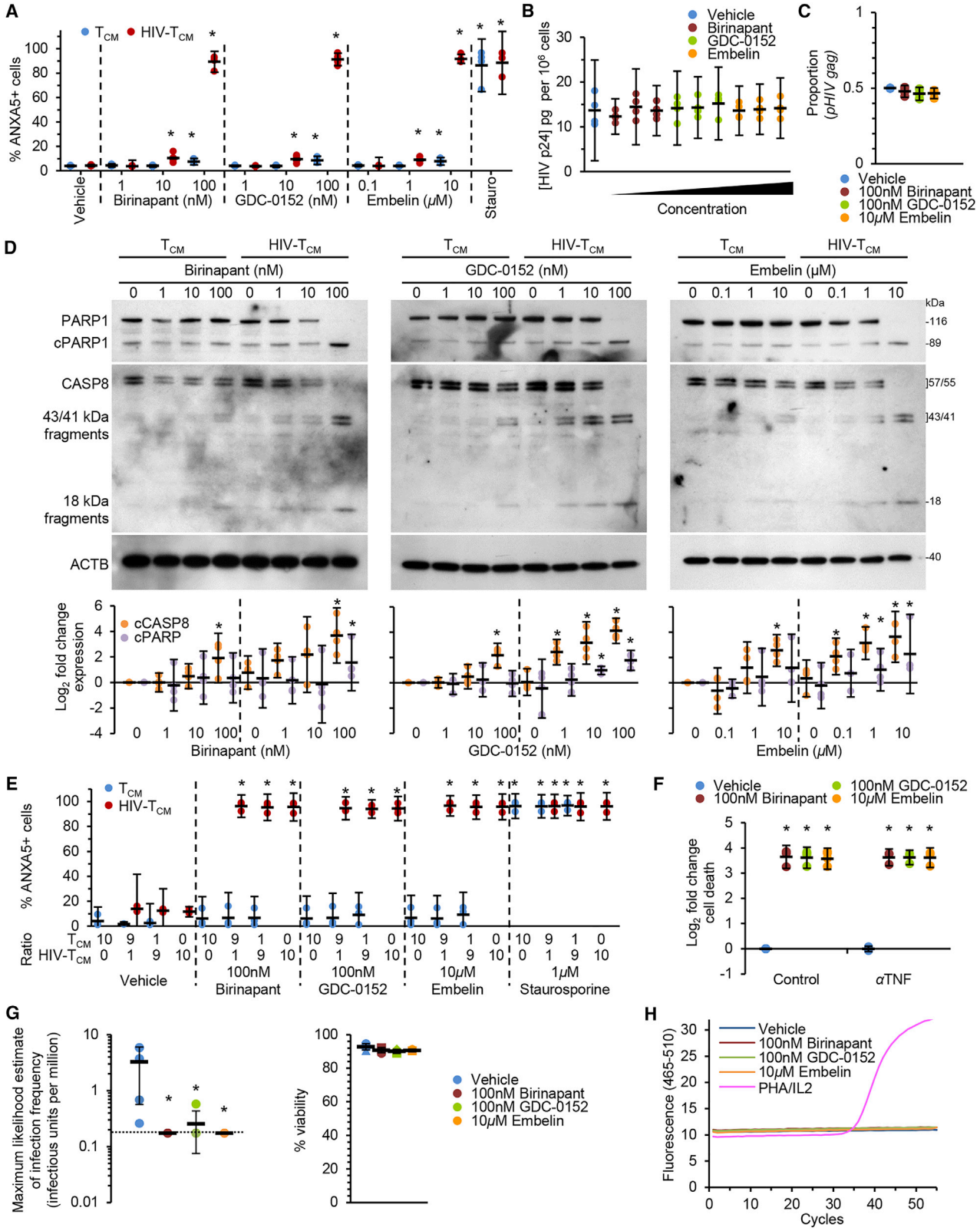

Figure 3. SMAC Mimetics Preferentially Induce Cell Death in HIV-T_{CM}

(A) T_{CM} and HIV-T_{CM} were treated with SM or 1 μM staurosporine (Stauro) for 24 hr, harvested, and stained with annexin-V (ANXA5) and PI. Representative dot plots are shown in Figure S3. The frequency of ANXA5-positive or ANXA5/PI-positive labeling is illustrated as a plot. Similar results were obtained using a cell

(legend continued on next page)

and FAS are upregulated in HIV-T_{CM}, and SM treatment degrades XIAP and BIRC2, we examined the ability of SM to induce cell death in HIV-T_{CM} and T_{CM}. All SM induced cell death in A3.01, ACH-2, T_{CM}, and HIV-T_{CM} in a dose-dependent manner over 24 hr (Figures 3A, S3, and S4A–S4C). Neither HIV-T_{CM} nor T_{CM} were sensitive to SM at the lowest concentrations tested. However, we started to observe significant cell death in HIV-T_{CM} at 10 nM birinapant, 10 nM GDC-0152, and 1 μM embelin. This cytotoxic effect was amplified at 100 nM birinapant, 100 nM GDC-0152, and 10 μM embelin, at which point cell death was approaching 90% and was similar to 1 μM staurosporine treatment. Conversely, we observed no cytotoxic effect in T_{CM} until we used 100 nM birinapant, 100 nM GDC-0152, and 10 μM embelin, and, at these doses, cell death was just 3.5%–4.6% above basal levels. Importantly, we measured no SM-mediated increase in HIV p24 antigen release (Figure 3B) or cell-associated HIV *gag* RNA (Figure 3C), indicating that the SM were killing HIV-T_{CM} in the absence of increased virus production. SM also induced the dose-dependent proteolysis of poly(ADP-ribose) polymerase 1 (PARP1) into an 89 kDa fragment, a measure of apoptosis, in the HIV-T_{CM} but not in the T_{CM} (Figure 3D). Additionally, in T_{CM}, CASP8 cleavage only became significant at the highest concentrations tested, whereas HIV-T_{CM} displayed significant CASP8 cleavage after the lowest doses of GDC-0152 and embelin (Figure 3D).

To determine if the preferential killing of HIV-T_{CM} by SM was a direct effect on infected cells or secondary to toxic factors secreted into cell cultures, we examined a co-culture system in which we mixed HIV-T_{CM} with T_{CM} followed by exposure to SM. In these heterogeneous cultures, we observed no increase in cell death in either cell type in the absence of SM ($p > 0.14$; Figure 3E). When the cultures were mixed at a T_{CM}:HIV-T_{CM} ratio of 9:1, SM induced more than 90% of HIV-T_{CM} to undergo cell death ($p < 0.001$) in the absence of appreciable T_{CM} death ($p > 0.25$). When this ratio was reversed to 1:9, SM again induced significant (>90%) HIV-T_{CM} death ($p < 0.001$) but no significant T_{CM} death. Importantly, staurosporine induced similar levels of cell death in both the homogeneous and the heterogeneous populations. Despite observing cell death, there was no measurable change in integrated HIV DNA copy number per cell as the dying cells are still present and their integrated HIV DNA still quantifiable (Figure S4D), which is consistent with other studies (Yin et al., 2015). We then assessed whether the kinetics of killing uninfected T_{CM} are slower compared with HIV-T_{CM} by incubating the cells with birinapant for 96 hr. We observed no increase in cell death over this time, suggesting that at no point does T_{CM} undergo cell death in response to SM to the same extent as the HIV-T_{CM} (Figure S4E).

In leukemic cells, SM-treatment-induced expression of TNF is an important driver of SM-induced cell death (Petersen et al., 2007). Therefore, we blocked TNF signaling with a specific neutralizing antibody. Neutralization of TNF had no effect on SM-mediated cell death (Figures 3F and S4F–S4H). This correlated with our failure to detect the expression of TNFR on these cells and suggests that SM-mediated killing of HIV-T_{CM} is not dependent upon TNF expression.

Next, using cells collected from HIV-infected patients undergoing ART, we evaluated the ability of SM to eliminate resting CD4+ T cells latently infected with HIV, which would lead to a decrease in levels of inducible HIV. As hypothesized, 24 hr SM treatment of these cells led to a significant decrease in HIV p24 antigen expression in a viral outgrowth assay, relative to vehicle-treated controls in the absence of globally increased cell death (Figure 3G). Importantly, SM treatment did not result in a reversal of latency, as we were unable to detect viral reactivation as measured by HIV *gag* RT-qPCR after 24 hr SM treatment in these cells (Figure 3H).

SM Induce Apoptosis in HIV-Infected CD4+ T Cells

Annexin-V (ANXA5)/propidium iodide (PI) double-positive staining is not exclusive to classic apoptosis. Upon necroptosis/programmed necrosis induction, cells can be stained double positive, as their plasma membrane is damaged allowing PI and ANXA5 to penetrate the cell and bind to the phosphatidylserine located on the inner leaflet of the membrane. Therefore, we examined the effect of SM on HIV-T_{CM} in the presence of pharmacological inhibitors of apoptosis (pan-caspase inhibitor z-VAD-FMK), autophagy (PI3K inhibitor wortmannin), and/or necroptosis (RIPK1 inhibitor necrostatin-1). Rescue from SM-induced cell death varied among donors, but we detected similar induced cell death patterns for birinapant, embelin, and GDC-0152 (Figure 4A). None of the samples tested showed a purely apoptotic phenotype, but all required either wortmannin or simultaneous application of z-VAD-FMK and necrostatin-1

death ELISA and are shown as a comparison in Figure S4B. DNA was extracted from HIV-T_{CM} for Alu-long terminal repeat (LTR)-based nested qPCR and is shown in Figure S4C n = 4.

(B) ELISA performed for HIV p24 antigen in supernatants from cells treated in (A). n = 4.

(C) RT-qPCR performed for extracellular release of HIV *gag* mRNA from cells treated in (A). n = 4.

(D) T_{CM} and HIV-T_{CM} were treated with SM for 24 hr. *Top*, representative western blots of PARP1 and CASP8 cleavage (cPARP1 and cCASP8) using antibody to PARP1, CASP8, and ACTB. *Bottom*, densitometric analysis of blots, n = 4.

(E) T_{CM} and HIV-T_{CM} were fluorescently labeled, mixed at different ratios, treated with SM or staurosporine for 24 hr, harvested, and stained with ANXA5 and PI; the frequency of ANXA5-positive or ANXA5/PI-positive labeling in the different populations was recorded by flow cytometry and illustrated as a dot plot. DNA was extracted from cultures for Alu-LTR-based nested qPCR and is shown Figure S4D n = 4.

(F) HIV-T_{CM} were pretreated with vehicle control or TNF neutralizing antibody 2 hr before incubation with SM for 24 hr. Cell death was measured using a cell death ELISA. n = 4.

(G) Resting CD4+ T cells were isolated from HIV-infected donors on suppressive ART, viral load <20 copies mL^{-1} and CD4+ count >400 μL^{-1} for at least 6 months. Cells were treated with SM for 24 hr. Left, using the viral outgrowth assay, the frequency of latently infected cells was measured at day 14 with an HIV p24 antigen ELISA. The dotted line indicates the detection limit of the assay. Right, viability of cells after the 24 hr SM treatment. n = 5.

(H) Resting CD4+ T cells isolated from HIV-infected donors on suppressive ART (viral load <20 copies mL^{-1} and CD4+ count >400 μL^{-1} for at least 6 months) were treated with SM or PHA/IL2 for 24 hr. RT-qPCR performed for HIV *gag* in supernatants from cells. Representative samples shown. n = 4.

Each symbol represents one donor. Error bars show mean ± 95% confidence interval. For (G), error bars show mean ± SD. *$p < 0.05$ determined by Student's t test.

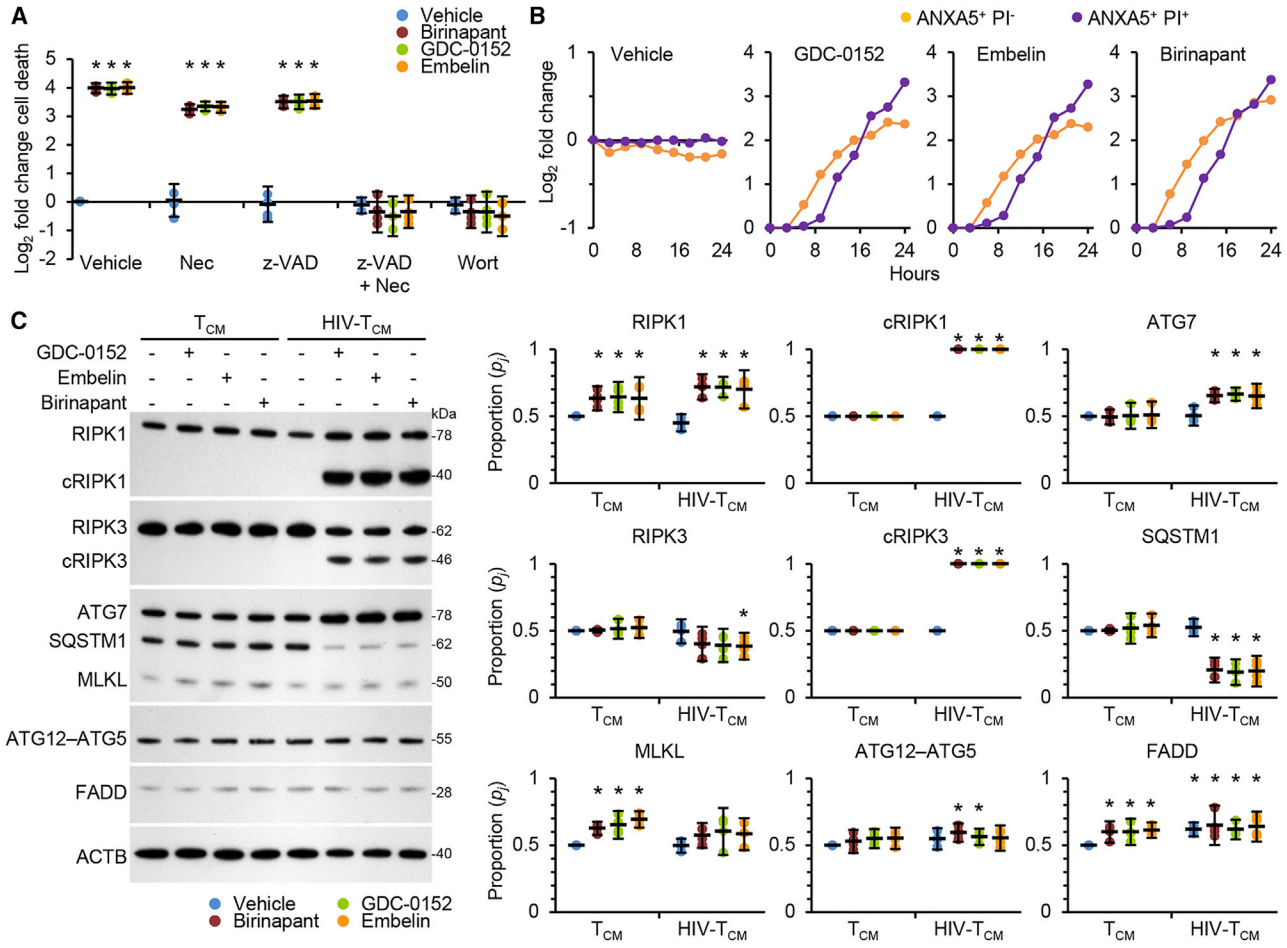

Figure 4. SMAC Mimetics Promote Cell Death via Apoptosis

(A) HIV-T_{CM} were pretreated with necrostatin-1 (Nec), z-VAD-fmk (z-VAD), wortmannin (Wort), or vehicle control for 2 hr. Cell death was measured 24 hr after subsequent 100 nM birinapant, 100 nM GDC-0152, or 10 μM embelin treatment using a cell death ELISA. n = 4.

(B) HIV-T_{CM} were exposed to 100 nM birinapant, 100 nM GDC-0152, or 10 μM embelin. Every 3 hr for 24 hr, cells were harvested, stained with ANXA5 and PI, and the frequency of ANXA5-positive or ANXA5/PI-positive labeling was recorded by flow cytometry. Data are the means of a representative donor.

(C) T_{CM} and HIV-T_{CM} were treated with 100 nM birinapant, 100 nM GDC-0152, 10 μM embelin, or vehicle for 24 hr. Left, representative western blots of ATG7, ATG12–ATG5, FADD, MLKL, RIPK1, cleaved RIPK1 (cRIPK1), RIPK3, cleaved RIPK3 (cRIPK3), and SQSTM1 in T_{CM} and HIV-T_{CM}. Right, densitometric analysis of blots. n = 4.

For (A) and (C), each symbol represents one donor. Error bars show mean ± 95% confidence interval. *p < 0.05 determined by Student's t test.

to arrest SM-induced cell death (Figure 4A). Although complete rescue did not occur, inhibition of either RIPK1 or caspases alone actually increased cell viability post SM treatment, suggesting that cells switch to the alternative pathway when a single pathway is inhibited. Since both the pan-caspase inhibitor and the RIPK1 inhibitor increased cell viability after SM treatment, we next performed temporal staining. All SM induced ANXA5 positivity first (apoptosis) but little dual PI positivity (necroptosis) at early time points, with temporally coincident staining commencing ~9 hr post SM treatment indicating a classic apoptotic phenotype (Figure 4B).

As FAS, FASLG (both membrane-bound and soluble), XIAP, and BIRC2 are upregulated in HIV-T_{CM}, we next tested whether varying expression of key components of the apoptotic and necroptotic response might contribute to the differential response to SM in T_{CM} and HIV-T_{CM}. We observed no consistent correlation of CASP8, RIPK1, RIPK3, FADD, or mixed lineage kinase domain like pseudokinase (MLKL) protein expression with sensitivity to SM in either T_{CM} or HIV-T_{CM} (Figure 4C). Moreover, there was no difference in basal expression of SQSTM1, ATG5, or ATG7. Collectively, these data indicate that HIV-T_{CM} cell death in response to SM correlates with (1) HIV-induced expression of LC3B-II, BECN1, FAS, FASLG, XIAP, and BIRC2; (2) degradation of BIRC2 and XIAP; and (3) an increase in autophagy.

In the next series of experiments, we assessed the effect of SM on these same key players of the apoptotic and necroptotic response. At the doses tested, there was cleavage of RIPK1 and RIPK3 and an increase in the expression of ATG7 in HIV-T_{CM} but not in T_{CM} (Figure 4C). The cleavage of RIPK1 and RIPK3 is consistent with reports that RIPK1 and RIPK3 are targets of CASP8 cleavage, and thus, as CASP8 is activated, RIPK1 and RIPK3 are cleaved (Moquin and Chan, 2010). Conversely,

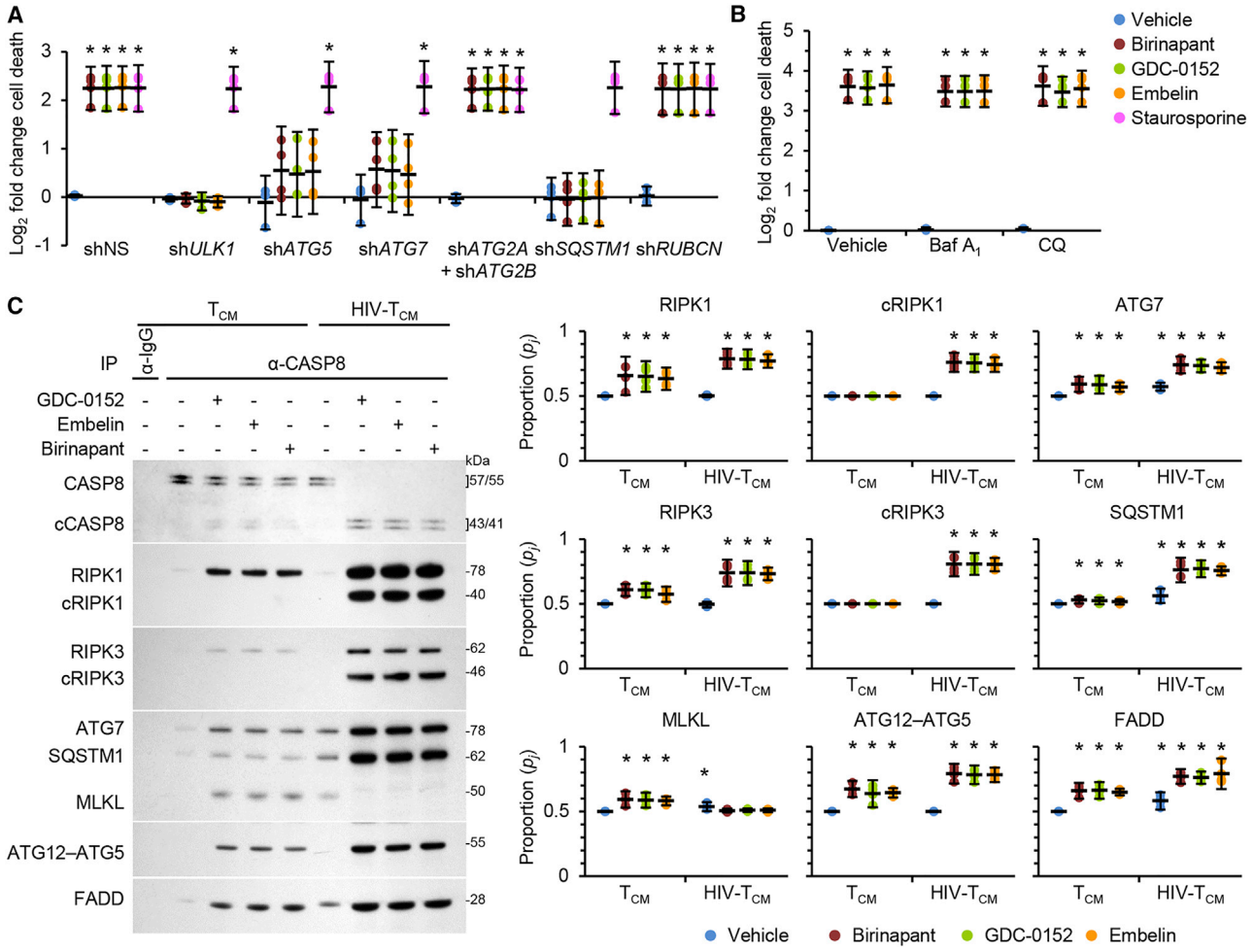

Figure 5. SMAC Mimetics Promote Cell Death via the Formation of a CASP8-Activating Platform

(A) HIV-T_{CM} simultaneous transduced with *ATG2A* and *ATG2B* short hairpin RNA (shRNA) (sh*ATG2A/B*), *ATG5* shRNA (sh*ATG5*), *ATG7* (sh*ATG7*), *RUBCN* (sh*RUBCN*), *SQSTM1* (sh*SQSTM1*), *ULK1* (sh*ULK1*), or scrambled shRNA (shNS) were incubated with 100 nM birinapant, 100 nM GDC-0152, 10 μM embelin, or vehicle. Cell death was measured after 24 hr using a cell death ELISA. n = 4. Relative silencing efficiencies are shown in Figure S5A.

(B) HIV-T_{CM} were pretreated with vehicle, bafilomycin A_1 (Baf A1), or chloroquine (CQ) before incubation with 100 nM birinapant, 100 nM GDC-0152, or 10 μM embelin for 24 hr. Cell death was measured using a cell death ELISA. n = 4. Autophagy inhibition efficiencies are demonstrated in Figures S2A and S5B.

(C) T_{CM} and HIV-T_{CM} were treated with 100 nM birinapant, 100 nM GDC-0152, or 10 μM embelin for 24 hr. Cells were lysed and CASP8 was immunoprecipitated (IP). The presence of ATG7, ATG12–ATG5, FADD, MLKL, cRIPK1, RIPK3, cRIPK3, and SQSTM1 and CASP8 was assayed by western blot. Left, representative western blots. Right, densitometric analysis of blots. n = 4.

Each symbol represents one donor. Error bars show mean ± 95% confidence interval. *p < 0.05 determined by Student's t test.

MLKL, an important necroptosis mediator (Yoon et al., 2016), was increased in T_{CM} but not in HIV-T_{CM} (Figure 4C). These data indicate that the SM induce apoptosis, but, when CASP8 is inhibited, the necroptotic pathway is invoked.

SM-Induced Apoptosis Is Dependent upon the Autophagy Machinery

Since wortmannin, an inhibitor of early stages of autophagy, inhibited SM-induced apoptosis despite IAP degradation, we next tested how autophagy affects SM-mediated cell death in HIV-T_{CM}. In these experiments, inhibition of the autophagy conjugation cascades with RNAi for *ULK1* (unc-51-like autophagy activating kinase 1), *ATG5*, *ATG7*, or *SQSTM1* (Figure S5A) led to increased cell viability in the presence of SM (Figure 5A). In contrast, we observed no effect on SM-induced death by blocking autophagic flux using either simultaneous RNAi for *ATG2A* and *ATG2B* (*ATG2A/B*), which causes the accumulation of immature unclosed autophagosomal structures (Figure 5A), or the inhibition of autophagosome-lysosome fusion using either chloroquine or bafilomycin A_1 (Figure 5B). Importantly, we observed no effect on SM-induced death with the inhibition of LC3-associated phagocytosis using RUN and cysteine rich domain containing beclin 1 interacting protein (RUBCN) silencing. Collectively, these data suggest that neither fully formed autophagosomes or autophagy-mediated degradation of cargo is required to induce cell death in response to SM because, if this were the case, a similar effect on cell death would occur regardless of autophagy stage inhibited.

A complex including RIPK1, CASP8, and FADD (a ripoptosome) is generated following the loss of BIRC2 and subsequent RIPK1 ubiquitination and degradation (Feoktistova et al., 2011; Tenev et al., 2011). Having observed that the induction, but not the completion, of autophagy is required for SM-mediated killing of HIV-T_{CM}, we next examined whether the autophagy machinery might provide a scaffold for the formation of a ripoptosome-like death-inducing signaling complex (DISC) composed of RIPK1, RIPK3, FADD, and CASP8 using co-immunoprecipitation. While the ripoptosome-like complex proteins RIPK1, RIPK3, and FADD co-immunoprecipitated with CASP8 in T_{CM} and HIV-T_{CM}, MLKL only co-immunoprecipitated with CASP8 in T_{CM} (Figure 5C). In both T_{CM} and HIV-T_{CM}, proteins involved in early to middle stages of autophagy, including ATG5, ATG7, and SQSTM1, co-immunoprecipitated with CASP8 (Figure 5C). However, proteins that are important for earlier signaling in the autophagy process (BECN1 and ULK1) and those involved in later steps when autophagosomes fuse with lysosomes (syntaxin 17 [STX17] and lysosomal-associated membrane protein 1 [LAMP1]) did not co-immunoprecipitate with CASP8.

We next assessed whether autophagy proteins are required for efficient SM-mediated ripoptosome-like complex formation and activation in HIV-T_{CM} using RNAi. *ATG5* silencing abrogated the SM-mediated CASP8, RIPK1, and RIPK3 cleavage (Figures 6A and S6A) and induced a significant negative change in RIPK1 co-immunoprecipitation with CASP8, RIPK3, ATG7, FADD, and SQSTM1 (Figures 6B and S6B). Similarly, *ATG7* silencing abrogated the SM-mediated CASP8, RIPK1, and RIPK3 cleavage (Figures 6A and S6A), and pull-down of RIPK1 displayed a significant negative change in RIPK1 association with CASP8, RIPK3, ATG7, FADD, and SQSTM1 (Figures 6B and S6B). Notably, MLKL did not associate with RIPK1 after either RNAi. As RIPK1 directly interacts with SQSTM1 (Sanz et al., 1999), we also silenced *SQSTM1* and found a significant reduction in CASP8, RIPK1, and RIPK3 cleavage (Figures 6C and S7A). Moreover, RNAi for *SQSTM1* significantly reduced the SM-mediated association of RIPK1 with CASP8, RIPK3, ATG7, FADD, and ATG5 (Figures 6D and S7B). These findings correspond to the increase in cell viability observed upon SM treatment of *SQSTM1* silenced cells (Figure 5A). These data indicate that RIPK1 requires SQSTM1 for the assembly and activation of the ripoptosome-like complex after SM treatment of HIV-T_{CM}.

As RIPK1 directly interacts with SQSTM1, it is possible that ripoptosome-like complex components translocate to autophagosomal membranes. Therefore, we determined the stage of autophagosome formation at which ripoptosome-like complexes localize to autophagic structures by analyzing membranes in *ATG2A/B* silenced cells using differential centrifugation with LC3B-II and SQSTM1 used as markers of autophagosome membranes and autophagy substrates, respectively (Velikkakath et al., 2012). In the control cells and in the absence of birinapant, LC3B (as LC3B-I), SQSTM1, FADD, and RIPK1 were located primarily in the cytosol, as indicated by their presence in the high-speed supernatant (HSS) fraction (Figure 7A). However, in the presence of birinapant and bafilomycin A_1, LC3B accumulated, together with SQSTM1, in the low-speed pellet (LSP) and was resistant to proteinase K but sensitive to Triton X-100/proteinase K, indicating that the LC3B and SQSTM1 collected in this fraction were enclosed by autophagosomes. Conversely, SQSTM1, RIPK1, cleaved RIPK1, and FADD accumulated in the high-speed pellet (HSP), which was sensitive to both proteinase K and Triton X-100/proteinase K, indicating that these were not enclosed structures (Figure 7A). In *ATG2A/B* silenced cells, proteinase K-sensitive LC3B-II and SQSTM1 accumulated in the HSP fraction in the absence of birinapant and bafilomycin A_1. In the presence of birinapant and bafilomycin A_1, they accumulated in both the LSP and HSP fractions, while proteinase K-sensitive RIPK1, cleaved RIPK1, and FADD were present only in the HSP fraction (Figure 7A). Collectively, this suggests that ATG2A and ATG2B are required for complete closure of autophagosomes, as LC3B-II-positive structures accumulate in their absence (Velikkakath et al., 2012), and that RIPK1 and FADD do not translocate into closed autophagosomes after SM treatment.

DISCUSSION

To date, efforts to purge the latent HIV reservoir have often included a "shock and kill" strategy. This approach endeavors to reactivate viral production from latently infected reservoir cells (the shock), followed by clearance of these cells through a combination of viral and cell-mediated cytotoxicity (the kill) while ART prevents subsequent rounds of infection. Although latency reactivating agents have shown promise in cell lines, most are unable to induce substantive viral transcription in primary resting CD4+ T cells from patients on suppressive ART (reviewed in Spivak and Planelles, 2016), and reactivation from latency is often insufficient to induce cell death (Walker-Sperling et al., 2016). Therefore, we used an alternative strategy designed to activate cell death pathways selectively in HIV-infected cells while sparing uninfected cells. We specifically targeted a cell death pathway because HIV has evolved mechanisms to evade apoptosis to promote cell survival. Importantly, the SM tested failed to reactivate viral production from latently infected reservoir CD4+ T cells collected from HIV-infected patients undergoing ART. These findings are in agreement with Pache et al. (2015), who showed that the SM SBI-0637142 and LCL161 also failed to activate latent provirus in resting CD4+ T cells collected from HIV-infected patients undergoing ART.

Our data suggest that the selective killing of HIV-T_{CM} by SM is dependent on the induction of autophagy and the translocation and interaction of FADD and the CASP8 homocomplex with ATG5 and SQSTM1. Autophagy proteins thus serve as a scaffold for the efficient assembly of a cytosolic DISC involving RIPK1 and RIPK3 that initiates apoptosis, connecting the induction of autophagy to apoptotic cell death (Figure 7B). Several independent pieces of evidence support this conclusion: (1) each of the SM studied induced autophagy, although analysis of SM-induced IAP degradation indicate that SM are capable of inducing apoptosis at concentrations that resulted in the complete autophagy independent-degradation of both XIAP and BIRC2; (2) RNAi for *ATG5*, *ATG7*, *SQSTM1*, or *ULK1*, and pharmacological inhibition of early autophagy events, abrogated the formation of the cytosolic DISC and inhibited subsequent CASP8 activation and cell death; and (3) neither simultaneous

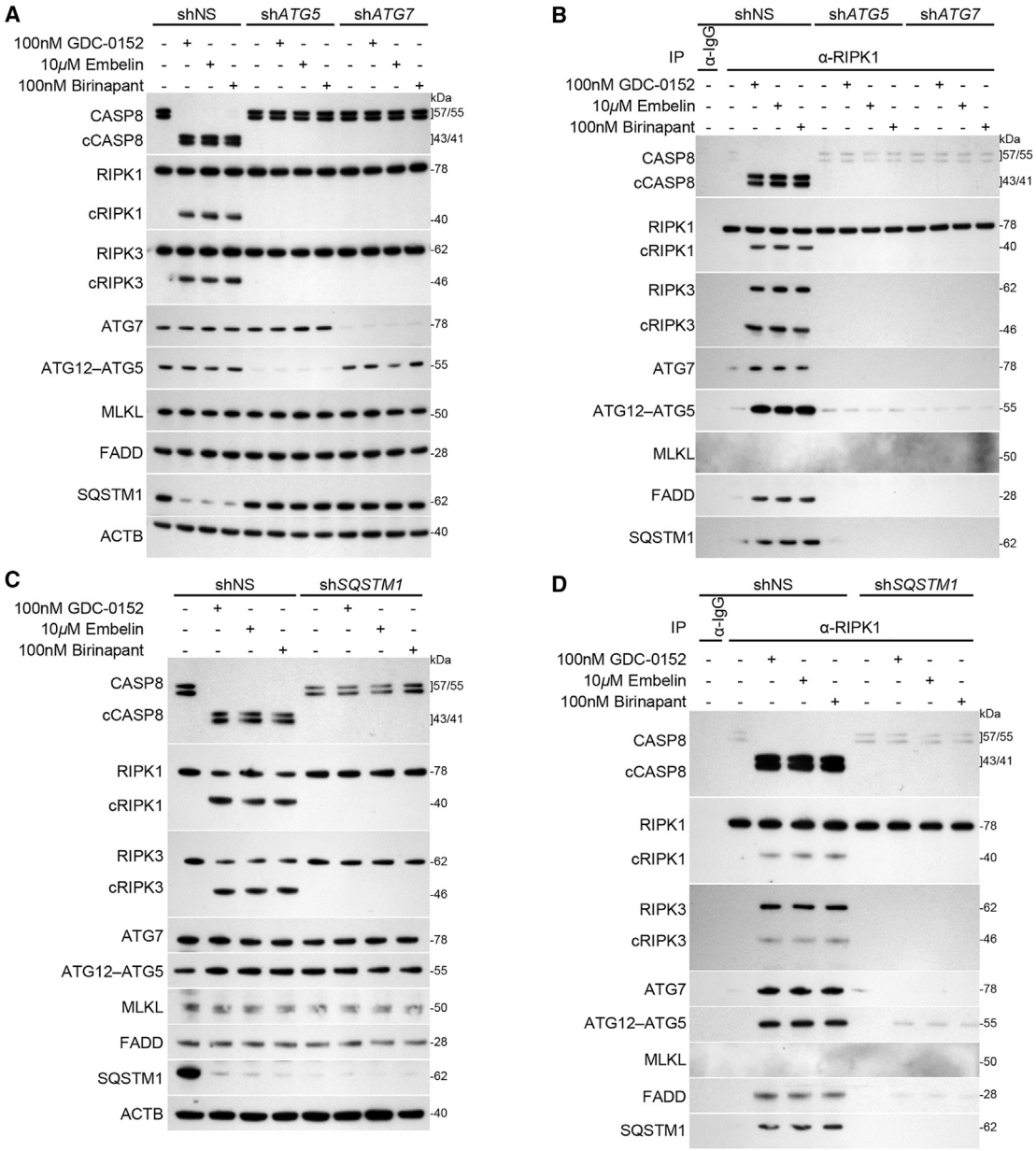

Figure 6. SMAC Mimetics Promote Cell Death via the Autophagy-Dependent Formation of a CASP8-Activating Platform Involving SQSTM1

(A) HIV-T_{CM} transduced with sh*ATG5*, sh*ATG7*, or shNS were incubated with birinapant, GDC-0152, or embelin for 24 hr then lysed. Representative western blots of ATG7, ATG12–ATG5, FADD, MLKL, cRIPK1, RIPK3, cRIPK3, and SQSTM1. Densitometric analysis of blots are presented in Figure S6A n = 4.

(B) RIPK1 was IP from cell lysates in (A). The presence of ATG7, ATG12–ATG5, FADD, MLKL, RIPK1, RIPK3, and SQSTM1 and CASP8 was assayed by western blot. Densitometric analyses of blots are shown in Figure S6B n = 4.

(C) HIV-T_{CM} transduced with *SQSTM1* shRNA (sh*SQSTM1*), or shNS were incubated with birinapant, GDC-0152, or embelin for 24 hr then lysed. Representative western blots of ATG7, ATG12–ATG5, FADD, MLKL, cRIPK1, RIPK3, cRIPK3, and SQSTM1. Densitometric analysis of blots are presented in Figure S7A n = 4.

(D) RIPK1 was IP from cell lysates in (C). The presence of ATG7, ATG12–ATG5, FADD, MLKL, RIPK1, RIPK3, and SQSTM1 and CASP8 was assayed by western blot. Densitometric analyses of blots are shown in Figure S7B n = 4.

silencing of *ATG2A* and *ATG2B* nor the pharmacological inhibition of autophagosome-lysosome fusion protected cells from SM-mediated cell death. These data suggest that the SM-mediated autophagy does not influence cell death through the selective degradation of pro- or anti-apoptotic proteins, since, if the autophagic process were important, cell death would occur regardless of which stage of autophagy is inhibited. Rather, our data indicate that the induction of autophagy affects cell survival. In this regard, self-oligomerized SQSTM1 can localize and recruit RIPK1 to the endoplasmic reticulum-associated autophagosome formation site independently of LC3 and is retained as autophagosomes mature (Goodall et al., 2016; Itakura and Mizushima, 2011), while FADD is involved in tethering CASP8 and RIPK1 to autophagosomal

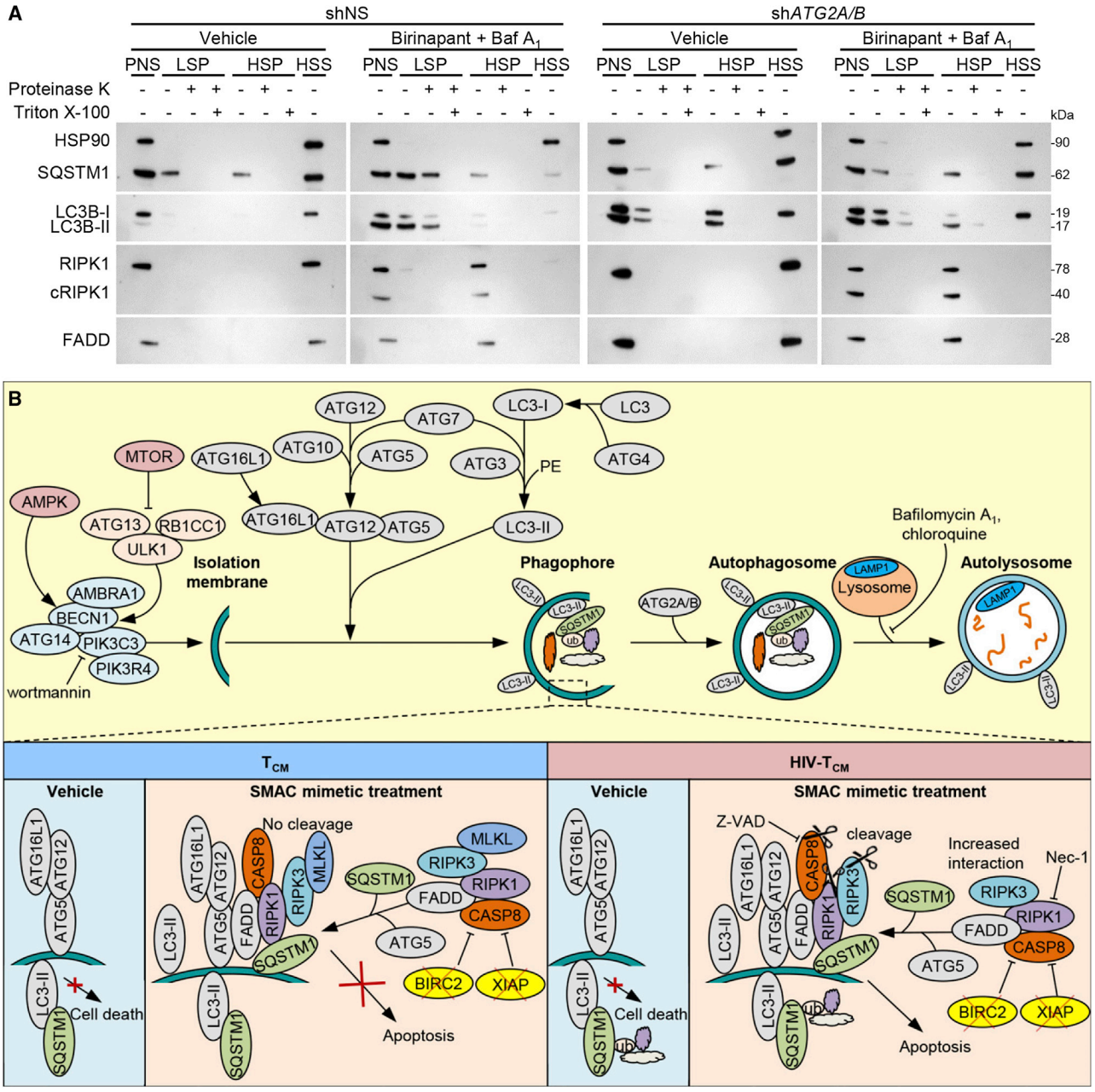

Figure 7. SMAC Mimetics Promote Cell Death via the Autophagy-Dependent Formation of a CASP8-Activating Platform on Autophagosomal Membranes

(A) HIV-T_{CM} simultaneously transduced with a mixture of shRNA against *ATG2A* and *ATG2B* (sh*ATG2A/B*) or shNS were cultured in growth media supplemented with both 100 nM birinapant and 200 nM bafilomycin A_1 ($Baf A_1$) or vehicle for 2 hr. The post-nuclear supernatant (PNS) was separated into an LSP, an HSP, and a HSS fraction and subjected to western blotting. The sub-fractions were treated with proteinase K with or without Triton X-100. Representative western blots are shown. n = 4. Analysis of silencing is shown in Figure S5A.

(B) Selected aspects of the key factors involved in the molecular regulation of autophagy and their roles in SM-mediated apoptosis of HIV-T_{CM}. Ub, ubiquitin; Nec-1, necrostatin-1; Z-VAD, Z-VAD-fmk.

membranes via ATG5 (Bell et al., 2008). Here, we show that, following SM treatment of HIV-T_{CM}, SQSTM1 coimmunoprecipitates with ATG5, CASP8, FADD, RIPK1, and RIPK3, that this is dependent upon the upstream proteins ATG5 and ATG7, and that both RIPK1 and FADD co-localize to the HSP with SQSTM1, defining a mechanism for how autophagy is involved in the control of cell survival or death.

The observed increase in autophagic markers in HIV-T_{CM} is consistent with the hypothesis that HIV utilizes autophagosomal membranes as a scaffold for Gag processing and the production

of nascent virions, while controlling the antiviral proteolytic and degradative late stages of autophagy to avoid its own degradation (Borel et al., 2015; Campbell et al., 2015; Kyei et al., 2009). These data are also consistent with the findings that autophagic flux is significantly impaired in CD4+ T cells from HIV-infected individuals, and peripheral blood mononuclear cells (PBMCs) from elite controllers contain significantly more autophagic vesicles and express more autophagic markers than normal progressors (Gomez-Mora et al., 2017). Additionally, PBMCs from elite controllers were more responsive to sirolimus treatment, leading to an enhanced autophagic response and a greater reduction in virus production, illustrating the importance of autophagy in the cellular antiviral response (Nardacci et al., 2014).

In summary, our findings identify a molecular mechanism whereby we can selectively induce apoptosis of HIV-T_{CM} through the assembly of a ripoptosome-like DISC involving autophagy machinery without viral reactivation while sparing uninfected cells. These findings suggest that DIABLO/SMAC mimetics can play an important role in the development of a cure strategy for HIV.

STAR★METHODS

Detailed methods are provided in the online version of this paper and include the following:

- KEY RESOURCES TABLE
- CONTACT FOR REAGENT AND RESOURCE SHARING
- EXPERIMENTAL MODEL AND SUBJECT DETAILS
  - Cell Culture
  - Primary Human Cells
  - Ethical Statement
  - Virus
- METHOD DETAILS
  - Establishment of Resting, HIV Infected CD4+ T Cells
  - Latent HIV Limiting Dilution Co-culture Assay
  - Flow Cytometry
  - Lactate Dehydrogenase Activity
  - Chemicals
  - Anti-TNF Neutralization Assay
  - shRNA Transduction
  - Western Blotting
  - Subcellular Fractionation and Proteinase K Treatment
  - Quantitative Real-Time PCR
  - Statistics

SUPPLEMENTAL INFORMATION

Supplemental Information includes seven figures and one table and can be found with this article online at https://doi.org/10.1016/j.chom.2018.09.007.

ACKNOWLEDGMENTS

This work was supported, in whole or in part, by the National Institute of Neurological Disorders and Stroke of the NIH (www.ninds.nih.gov) (R01 NS084912 and R01 NS104015 to S.A.S.), the California HIV/AIDS Research Program (www.californiaaidsresearch.org) (ID12-SD-255 to G.R.C.), and the International Maternal Pediatric Adolescent AIDS Clinical Trials Network (impaactnetwork.org). Overall support for the International Maternal Pediatric Adolescent AIDS Clinical Trials (IMPAACT) Network was provided by the National Institute of Allergy and Infectious Diseases (NIAID) of the NIH under award numbers UM1AI068632 (IMPAACT LOC), UM1AI068616 (IMPAACT SDMC), and UM1AI106716 (IMPAACT LC), with co-funding from the Eunice Kennedy Shriver National Institute of Child Health and Human Development (NICHD) and the National Institute of Mental Health (NIMH). The content is solely the responsibility of the authors and does not necessarily represent the official views of the NIH. The funders had no role in study design, data collection and analysis, decision to publish, or preparation of the manuscript.

AUTHOR CONTRIBUTIONS

G.R.C. and R.S.B. conducted and analyzed most of the experiments. Y.-L.C. conducted and analyzed all PCR for HIV integrated DNA. R.N.T. conducted and analyzed all other PCR experiments. S.A.S. and G.R.C. secured funding. G.R.C. conceived of the study; designed the experiments; and, together with S.A.S., wrote the manuscript.

DECLARATION OF INTERESTS

The authors declare no competing interests.

Received: April 4, 2018
Revised: June 15, 2018
Accepted: September 11, 2018
Published: October 18, 2018

REFERENCES

Adachi, A., Gendelman, H.E., Koenig, S., Folks, T., Willey, R., Rabson, A., and Martin, M.A. (1986). Production of acquired immunodeficiency syndrome-associated retrovirus in human and nonhuman cells transfected with an infectious molecular clone. J. Virol. *59*, 284–291.

Amaravadi, R.K., Schilder, R.J., Martin, L.P., Levin, M., Graham, M.A., Weng, D.E., and Adjei, A.A. (2015). A phase I study of the SMAC-mimetic birinapant in adults with refractory solid tumors or lymphoma. Mol. Cancer Ther. *14*, 2569–2575.

Bell, B.D., Leverrier, S., Weist, B.M., Newton, R.H., Arechiga, A.F., Luhrs, K.A., Morrissette, N.S., and Walsh, C.M. (2008). FADD and caspase-8 control the outcome of autophagic signaling in proliferating T cells. Proc. Natl. Acad. Sci. U S A *105*, 16677–16682.

Bergemann, T.L., and Wilson, J. (2011). Proportion statistics to detect differentially expressed genes: a comparison with log-ratio statistics. BMC Bioinformatics *12*, 228.

Berro, R., de la Fuente, C., Klase, Z., Kehn, K., Parvin, L., Pumfery, A., Agbottah, E., Vertes, A., Nekhai, S., and Kashanchi, F. (2007). Identifying the membrane proteome of HIV-1 latently infected cells. J. Biol. Chem. *282*, 8207–8218.

Bertrand, M.J., Milutinovic, S., Dickson, K.M., Ho, W.C., Boudreault, A., Durkin, J., Gillard, J.W., Jaquith, J.B., Morris, S.J., and Barker, P.A. (2008). cIAP1 and cIAP2 facilitate cancer cell survival by functioning as E3 ligases that promote RIP1 ubiquitination. Mol. Cell *30*, 689–700.

Borel, S., Robert-Hebmann, V., Alfaisal, J., Jain, A., Faure, M., Espert, L., Chaloin, L., Paillart, J.C., Johansen, T., and Biard-Piechaczyk, M. (2015). HIV-1 viral infectivity factor interacts with microtubule-associated protein light chain 3 and inhibits autophagy. AIDS *29*, 275–286.

Busca, A., Saxena, M., and Kumar, A. (2012). Critical role for antiapoptotic Bcl-xL and Mcl-1 in human macrophage survival and cellular IAP1/2 (cIAP1/2) in resistance to HIV-Vpr-induced apoptosis. J. Biol. Chem. *287*, 15118–15133.

Butler, S.L., Hansen, M.S., and Bushman, F.D. (2001). A quantitative assay for HIV DNA integration in vivo. Nat. Med. *7*, 631–634.

Buttke, T.M., and Folks, T.M. (1992). Complete replacement of membrane cholesterol with 4,4',14-trimethyl sterols in a human T cell line defective in lanosterol demethylation. J. Biol. Chem. *267*, 8819–8826.

Campbell, G.R., Rawat, P., Bruckman, R.S., and Spector, S.A. (2015). Human immunodeficiency virus type 1 Nef inhibits autophagy through transcription factor EB sequestration. PLoS Pathog. *11*, e1005018.

Campbell, G.R., and Spector, S.A. (2008). CCL2 increases X4-tropic HIV-1 entry into resting CD4+ T cells. J. Biol. Chem. *283*, 30745–30753.

Campbell, G.R., and Spector, S.A. (2013). Inhibition of human immunodeficiency virus type-1 through autophagy. Curr. Opin. Microbiol. *16*, 349–354.

Campbell, G.R., Watkins, J.D., Loret, E.P., and Spector, S.A. (2011). Differential induction of rat neuronal excitotoxic cell death by human immunodeficiency virus type 1 clade B and C Tat proteins. AIDS Res. Hum. Retroviruses *27*, 647–654.

Clouse, K.A., Powell, D., Washington, I., Poli, G., Strebel, K., Farrar, W., Barstad, P., Kovacs, J., Fauci, A.S., and Folks, T.M. (1989). Monokine regulation of human immunodeficiency virus-1 expression in a chronically infected human T cell clone. J. Immunol. *142*, 431–438.

Dettenhofer, M., and Yu, X.F. (1999). Highly purified human immunodeficiency virus type 1 reveals a virtual absence of Vif in virions. J. Virol. *73*, 1460–1467.

Feoktistova, M., Geserick, P., Kellert, B., Dimitrova, D.P., Langlais, C., Hupe, M., Cain, K., MacFarlane, M., Hacker, G., and Leverkus, M. (2011). cIAPs block ripoptosome formation, a RIP1/caspase-8 containing intracellular cell death complex differentially regulated by cFLIP isoforms. Mol. Cell *43*, 449–463.

Fitzwalter, B.E., and Thorburn, A. (2015). Recent insights into cell death and autophagy. FEBS J. *282*, 4279–4288.

Flygare, J.A., Beresini, M., Budha, N., Chan, H., Chan, I.T., Cheeti, S., Cohen, F., Deshayes, K., Doerner, K., Eckhardt, S.G., et al. (2012). Discovery of a potent small-molecule antagonist of inhibitor of apoptosis (IAP) proteins and clinical candidate for the treatment of cancer (GDC-0152). J. Med. Chem. *55*, 4101–4113.

Folks, T.M., Clouse, K.A., Justement, J., Rabson, A., Duh, E., Kehrl, J.H., and Fauci, A.S. (1989). Tumor necrosis factor alpha induces expression of human immunodeficiency virus in a chronically infected T-cell clone. Proc. Natl. Acad. Sci. U S A *86*, 2365–2368.

Fulda, S. (2015). Promises and challenges of SMAC mimetics as cancer therapeutics. Clin. Cancer Res. *21*, 5030–5036.

Gao, Z., Tian, Y., Wang, J., Yin, Q., Wu, H., Li, Y.M., and Jiang, X. (2007). A dimeric Smac/diablo peptide directly relieves caspase-3 inhibition by XIAP. Dynamic and cooperative regulation of XIAP by Smac/Diablo. J. Biol. Chem. *282*, 30718–30727.

Gomez-Mora, E., Robert-Hebmann, V., Garcia, E., Massanella, M., Clotet, B., Cabrera, C., Blanco, J., and Biard-Piechaczyk, M. (2017). Brief report: impaired CD4 T-Cell response to autophagy in treated HIV-1-infected individuals. J. Acquir. Immune Defic. Syndr. *74*, 201–205.

Goodall, M.L., Fitzwalter, B.E., Zahedi, S., Wu, M., Rodriguez, D., Mulcahy-Levy, J.M., Green, D.R., Morgan, M., Cramer, S.D., and Thorburn, A. (2016). The autophagy machinery controls cell death switching between apoptosis and necroptosis. Dev. Cell *37*, 337–349.

Gorantla, S., Makarov, E., Finke-Dwyer, J., Castanedo, A., Holguin, A., Gebhart, C.L., Gendelman, H.E., and Poluektova, L. (2010). Links between progressive HIV-1 infection of humanized mice and viral neuropathogenesis. Am. J. Pathol. *177*, 2938–2949.

Graham, F.L., Smiley, J., Russell, W.C., and Nairn, R. (1977). Characteristics of a human cell line transformed by DNA from human adenovirus type 5. J. Gen. Virol. *36*, 59–74.

Gump, J.M., Staskiewicz, L., Morgan, M.J., Bamberg, A., Riches, D.W., and Thorburn, A. (2014). Autophagy variation within a cell population determines cell fate through selective degradation of Fap-1. Nat. Cell Biol *16*, 47–54.

He, J., Choe, S., Walker, R., Di Marzio, P., Morgan, D.O., and Landau, N.R. (1995). Human immunodeficiency virus type 1 viral protein R (Vpr) arrests cells in the G2 phase of the cell cycle by inhibiting p34cdc2 activity. J. Virol. *69*, 6705–6711.

Hermankova, M., Ray, S.C., Ruff, C., Powell-Davis, M., Ingersoll, R., D'Aquila, R.T., Quinn, T.C., Siliciano, J.D., Siliciano, R.F., and Persaud, D. (2001). HIV-1 drug resistance profiles in children and adults with viral load of <50 copies/ml receiving combination therapy. JAMA *286*, 196–207.

Itakura, E., and Mizushima, N. (2011). p62 Targeting to the autophagosome formation site requires self-oligomerization but not LC3 binding. J. Cell Biol. *192*, 17–27.

Japour, A.J., Mayers, D.L., Johnson, V.A., Kuritzkes, D.R., Beckett, L.A., Arduino, J.M., Lane, J., Black, R.J., Reichelderfer, P.S., D'Aquila, R.T., et al. (1993). Standardized peripheral blood mononuclear cell culture assay for determination of drug susceptibilities of clinical human immunodeficiency virus type 1 isolates. The RV-43 Study Group, the AIDS Clinical Trials Group Virology Committee Resistance Working Group. Antimicrob. Agents Chemother. *37*, 1095–1101.

Kara, N.Z., Toker, L., Agam, G., Anderson, G.W., Belmaker, R.H., and Einat, H. (2013). Trehalose induced antidepressant-like effects and autophagy enhancement in mice. Psychopharmacology (Berl) *229*, 367–375.

Klionsky, D.J., Abdelmohsen, K., Abe, A., Abedin, M.J., Abeliovich, H., Acevedo Arozena, A., Adachi, H., Adams, C.M., Adams, P.D., Adeli, K., et al. (2016). Guidelines for the use and interpretation of assays for monitoring autophagy (3rd edition). Autophagy *12*, 1–222.

Kyei, G.B., Dinkins, C., Davis, A.S., Roberts, E., Singh, S.B., Dong, C., Wu, L., Kominami, E., Ueno, T., Yamamoto, A., et al. (2009). Autophagy pathway intersects with HIV-1 biosynthesis and regulates viral yields in macrophages. J. Cell Biol. *186*, 255–268.

Laird, G.M., Rosenbloom, D.I., Lai, J., Siliciano, R.F., and Siliciano, J.D. (2016). Measuring the frequency of latent HIV-1 in resting CD4(+) T cells using a limiting dilution coculture assay. Methods Mol. Biol. *1354*, 239–253.

Lewin, S.R., Murray, J.M., Solomon, A., Wightman, F., Cameron, P.U., Purcell, D.J., Zaunders, J.J., Grey, P., Bloch, M., Smith, D., et al. (2008). Virologic determinants of success after structured treatment interruptions of antiretrovirals in acute HIV-1 infection. J. Acquir. Immune Defic. Syndr. *47*, 140–147.

Lin, F., Ghislat, G., Luo, S., Renna, M., Siddiqi, F., and Rubinsztein, D.C. (2015). XIAP and cIAP1 amplifications induce Beclin 1-dependent autophagy through NFkappaB activation. Hum. Mol. Genet. *24*, 2899–2913.

López-Huertas, M.R., Mateos, E., Sanchez Del Cojo, M., Gomez-Esquer, F., Diaz-Gil, G., Rodriguez-Mora, S., Lopez, J.A., Calvo, E., Lopez-Campos, G., Alcami, J., et al. (2013). The presence of HIV-1 Tat protein second exon delays fas protein-mediated apoptosis in CD4+ T lymphocytes: a potential mechanism for persistent viral production. J. Biol. Chem. *288*, 7626–7644.

MacKenzie, J., Wilson, K.S., Perry, J., Gallagher, A., and Jarrett, R.F. (2003). Association between simian virus 40 DNA and lymphoma in the United Kingdom. J. Natl. Cancer Inst. *95*, 1001–1003.

Marini, A., Harper, J.M., and Romerio, F. (2008). An in vitro system to model the establishment and reactivation of HIV-1 latency. J. Immunol. *181*, 7713–7720.

Matthews, N., and Neale, M.L. (1987). Cytotoxicity assays for tumor necrosis factor and lymphotoxin. In Lymphokines and Interferons: A Practical Approach, M.J. Clemens, A.G. Morris, and A.J.H. Gearing, eds. (Oxford University Press), pp. 221–225.

Moquin, D., and Chan, F.K. (2010). The molecular regulation of programmed necrotic cell injury. Trends Biochem. Sci. *35*, 434–441.

Nardacci, R., Amendola, A., Ciccosanti, F., Corazzari, M., Esposito, V., Vlassi, C., Taibi, C., Fimia, G.M., Del Nonno, F., Ippolito, G., et al. (2014). Autophagy plays an important role in the containment of HIV-1 in nonprogressor-infected patients. Autophagy *10*, 1167–1178.

Norman, J.M., Cohen, G.M., and Bampton, E.T. (2010). The in vitro cleavage of the hAtg proteins by cell death proteases. Autophagy *6*, 1042–1056.

Pache, L., Dutra, M.S., Spivak, A.M., Marlett, J.M., Murry, J.P., Hwang, Y., Maestre, A.M., Manganaro, L., Vamos, M., Teriete, P., et al. (2015). BIRC2/cIAP1 is a negative regulator of HIV-1 transcription and can be targeted by Smac mimetics to promote reversal of viral latency. Cell Host Microbe *18*, 345–353.

Petersen, S.L., Wang, L., Yalcin-Chin, A., Li, L., Peyton, M., Minna, J., Harran, P., and Wang, X. (2007). Autocrine TNFalpha signaling renders human cancer cells susceptible to Smac-mimetic-induced apoptosis. Cancer Cell *12*, 445–456.

Pfaffl, M.W. (2001). A new mathematical model for relative quantification in real-time RT-PCR. Nucleic Acids Res. *29*, e45.

Pinti, M., Pedrazzi, J., Benatti, F., Sorrentino, V., Nuzzo, C., Cavazzuti, V., Biswas, P., Petrusca, D.N., Mussini, C., De Rienzo, B., et al. (1999). Differential down-regulation of CD95 or CD95L in chronically HIV-infected cells

of monocytic or lymphocytic origin: cellular studies and molecular analysis by quantitative competitive RT-PCR. FEBS Lett. *458*, 209–214.

Ramratnam, B., Mittler, J.E., Zhang, L., Boden, D., Hurley, A., Fang, F., Macken, C.A., Perelson, A.S., Markowitz, M., and Ho, D.D. (2000). The decay of the latent reservoir of replication-competent HIV-1 is inversely correlated with the extent of residual viral replication during prolonged anti-retroviral therapy. Nat. Med. *6*, 82–85.

Saleh, S., Wightman, F., Ramanayake, S., Alexander, M., Kumar, N., Khoury, G., Pereira, C., Purcell, D., Cameron, P.U., and Lewin, S.R. (2011). Expression and reactivation of HIV in a chemokine induced model of HIV latency in primary resting CD4+ T cells. Retrovirology *8*, 80.

Sanz, L., Sanchez, P., Lallena, M.J., Diaz-Meco, M.T., and Moscat, J. (1999). The interaction of p62 with RIP links the atypical PKCs to NF-kappaB activation. EMBO J. *18*, 3044–3053.

Silvestris, F., Cafforio, P., Frassanito, M.A., Tucci, M., Romito, A., Nagata, S., and Dammacco, F. (1996). Overexpression of Fas antigen on T cells in advanced HIV-1 infection: differential ligation constantly induces apoptosis. AIDS *10*, 131–141.

Spivak, A.M., and Planelles, V. (2016). HIV-1 eradication: early trials (and tribulations). Trends Mol. Med. *22*, 10–27.

Tenev, T., Bianchi, K., Darding, M., Broemer, M., Langlais, C., Wallberg, F., Zachariou, A., Lopez, J., MacFarlane, M., Cain, K., et al. (2011). The ripoptosome, a signaling platform that assembles in response to genotoxic stress and loss of IAPs. Mol. Cell *43*, 432–448.

Thorburn, J., Andrysik, Z., Staskiewicz, L., Gump, J., Maycotte, P., Oberst, A., Green, D.R., Espinosa, J.M., and Thorburn, A. (2014). Autophagy controls the kinetics and extent of mitochondrial apoptosis by regulating PUMA levels. Cell Rep. *7*, 45–52.

Townson, J.R., Barcellos, L.F., and Nibbs, R.J. (2002). Gene copy number regulates the production of the human chemokine CCL3-L1. Eur. J. Immunol. *32*, 3016–3026.

Varfolomeev, E., Blankenship, J.W., Wayson, S.M., Fedorova, A.V., Kayagaki, N., Garg, P., Zobel, K., Dynek, J.N., Elliott, L.O., Wallweber, H.J., et al. (2007). IAP antagonists induce autoubiquitination of c-IAPs, NF-kappaB activation, and TNFalpha-dependent apoptosis. Cell *131*, 669–681.

Velikkakath, A.K., Nishimura, T., Oita, E., Ishihara, N., and Mizushima, N. (2012). Mammalian Atg2 proteins are essential for autophagosome formation and important for regulation of size and distribution of lipid droplets. Mol. Biol. Cell *23*, 896–909.

Vicenzi, E., Panina-Bodignon, P., Vallanti, G., Di Lucia, P., and Poli, G. (2002). Restricted replication of primary HIV-1 isolates using both CCR5 and CXCR4 in Th2 but not in Th1 CD4(+) T cells. J. Leukoc. Biol. *72*, 913–920.

Walker-Sperling, V.E., Pohlmeyer, C.W., Tarwater, P.M., and Blankson, J.N. (2016). The effect of latency reversal agents on primary CD8+ T cells: implications for shock and kill strategies for human immunodeficiency virus eradication. EBioMedicine *8*, 217–229.

Wang, X., Ragupathy, V., Zhao, J., and Hewlett, I. (2011). Molecules from apoptotic pathways modulate HIV-1 replication in Jurkat cells. Biochem. Biophys. Res. Commun. *414*, 20–24.

Wei, X., Decker, J.M., Liu, H., Zhang, Z., Arani, R.B., Kilby, J.M., Saag, M.S., Wu, X., Shaw, G.M., and Kappes, J.C. (2002). Emergence of resistant human immunodeficiency virus type 1 in patients receiving fusion inhibitor (T-20) monotherapy. Antimicrob. Agents Chemother. *46*, 1896–1905.

Wolf, D., Witte, V., Laffert, B., Blume, K., Stromer, E., Trapp, S., d'Aloja, P., Schurmann, A., and Baur, A.S. (2001). HIV-1 Nef associated PAK and PI3-kinases stimulate Akt-independent Bad-phosphorylation to induce anti-apoptotic signals. Nat. Med. *7*, 1217–1224.

Yin, Y., Zhang, S., Luo, H., Zhang, X., Geng, G., Li, J., Guo, X., Cai, W., Li, L., Liu, C., et al. (2015). Interleukin 7 up-regulates CD95 protein on CD4+ T cells by affecting mRNA alternative splicing: priming for a synergistic effect on HIV-1 reservoir maintenance. J. Biol. Chem. *290*, 35–45.

Yoon, S., Bogdanov, K., Kovalenko, A., and Wallach, D. (2016). Necroptosis is preceded by nuclear translocation of the signaling proteins that induce it. Cell Death Differ. *23*, 253–260.

Zutshi, U., Sharma, S.C., Kaul, J.L., and Atal, C.K. (1990). Kinetic fate of potassium embelate, a non-narcotic centrally acting analgesic after oral and intravenous administration. Pharmacology *40*, 179–184.

STAR★METHODS

KEY RESOURCES TABLE

REAGENT or RESOURCE	SOURCE	IDENTIFIER
Antibodies		
α-human STX17	abcam	Cat# ab116113, RRID:AB_10903821
α-human SQSTM1	abcam	Cat# ab56416, RRID:AB_945626
α-human TUBB	abcam	Cat# ab21058, RRID:AB_727045
α-human CD62L PE-CF594 (clone DREG-56)	BD Horizon	Cat# 562301, RRID:AB_11154409
α-human HLA-DR V500 (clone G46-6)	BD Horizon	Cat# 561224, RRID:AB_10563765
α-human MKI67 BV421 (clone B56)	BD Horizon	Cat# 562899, RRID:AB_2686897
α-human CD3 APC-H7 (clone SK7)	BD Pharmingen	Cat# 560176, RRID:AB_1645475
α-human CD4 Alexa Fluor 647 (clone RPA-T4)	BD Pharmingen	Cat# 557707, RRID:AB_396816
α-human CD4 PE (clone L200)	BD Pharmingen	Cat# 550630, RRID:AB_393790
α-human CD4 PerCP-Cy5.5 (clone RPA-T4)	BD Pharmingen	Cat# 560650, RRID:AB_1727476
α-human CD25 Alexa Fluor 700 (clone M-A251)	BD Pharmingen	Cat# 561398, RRID:AB_10643605
α-human CD45RO APC (clone UCHL1)	BD Pharmingen	Cat# 559865, RRID:AB_398673
α-human CD69 FITC (clone FN50)	BD Pharmingen	Cat# 555530, RRID:AB_395915
α-human CCR7 PerCP-Cy5.5 (clone 150503)	BD Pharmingen	Cat# 561144, RRID:AB_10562553
α-human ATG2A	Cell Signaling Technology	Cat# 15011, RRID:AB_2732797
α-human ATG5	Cell Signaling Technology	Cat# 2630S, RRID:AB_2062340
α-human ATG7	Cell Signaling Technology	Cat# 2631S, RRID:AB_2227783
α-human BECN1	Cell Signaling Technology	Cat# 3738, RRID:AB_490837
α-human BIRC2 (clone D5G9)	Cell Signaling Technology	Cat# 7065S, RRID:AB_10890862
α-human CASP8 (clone 1C12)	Cell Signaling Technology	Cat# 9746, RRID:AB_2275120
α-human FADD	Cell Signaling Technology	Cat# 2782, RRID:AB_2100484
α-human FAS (clone C18C12)	Cell Signaling Technology	Cat# 4233S, RRID:AB_2100359
α-human FASLG	Cell Signaling Technology	Cat# 4273, RRID:AB_2100652
α-human LAMP1 (clone C54H11)	Cell Signaling Technology	Cat# 3243S, RRID:AB_2134478
α-human MLKL (clone D2I6N)	Cell Signaling Technology	Cat# 14993, RRID:AB_2721822
α-human PARP1 (clone 46D11)	Cell Signaling Technology	Cat# 9532, RRID:AB_659884
α-human RIPK1 (clone D94C12)	Cell Signaling Technology	Cat# 3493, RRID:AB_2305314
α-human RIPK3 (clone D4G2A)	Cell Signaling Technology	Cat# 95702, RRID:AB_2721823
α-human TNF (clone D1B4)	Cell Signaling Technology	Cat# 7321S, RRID:AB_10925386
α-human ULK1 (clone D9D7)	Cell Signaling Technology	Cat# 6439S, RRID:AB_11178933
α-human HSP90 (clone C45G5)	Cell Signaling Technology	Cat# 4877, RRID:AB_2233307
α-human XIAP (clone 3B6)	Cell Signaling Technology	Cat# 2045, RRID:AB_2214866
α-human HLA-DR biotin (clone AC122)	Miltenyi Biotec	Cat# 130-099-627, RRID:AB_2661329
α-human MAP1LC3B	Novus Biologicals	Cat# NB100-2220, RRID:AB_10003146
α-human ACTB (clone AC74)	Sigma	Cat# A2228, RRID:AB_476697
α-human ATG2B	Sigma	Cat# HPA019665, RRID:AB_2274278
Bacterial and Virus Strains		
HIV-1 NL4-3 Infectious Molecular Clone (pNL4-3)	National Institute of Health – AIDS Reagent Program	Cat# 114
Biological Samples		
Human peripheral blood mononuclear cells (PBMC)	UC San Diego Health Sciences, San Diego, CA, USA	N/A
Human peripheral blood mononuclear cells (PBMC)	UCSD Mother-Child-Adolescent HIV Program, San Diego, CA, USA	N/A

(*Continued on next page*)

Continued

REAGENT or RESOURCE	SOURCE	IDENTIFIER
Chemicals, Peptides, and Recombinant Proteins		
Bafilomycin A1	Alfa Aesar	Cat# J61835
AmpliTaq Gold™ DNA Polymerase with Buffer II and MgCl2	Applied Biosystems	Cat# N8080241
GeneAmp dNTP Blend	Applied Biosystems	Cat# N8080260
Tropix CDP-Star	Applied Biosystems	Cat# T2146
Tropix Nitro-Block II	Applied Biosystems	Cat# T2184
Fixation and Permeabilization Solution	BD Biosciences	Cat# 554722
Perm/Wash Buffer	BD Biosciences	Cat# 554723
Enterotoxin type B from *Staphylococcus aureus*	Calbiochem	Cat# 324798
Ficoll-Paque PLUS	GE Healthcare	Cat# 17-1440-03
Dulbecco's PBS	Gibco	Cat# 14190250
Geneticin selective antibiotic (G418 sulfate)	Gibco	Cat# 10131027
Puromycin dihydrochloride	Gibco	Cat# A1113803
Secondary antibody solution alk-phosphatase conjugated (anti-mouse)	Invitrogen	Cat# WP20006
Secondary antibody solution alk-phosphatase conjugated (anti-rabbit)	Invitrogen	Cat# WP20007
WesternBreeze wash solution (16X)	Invitrogen	Cat# WB7003
Bafilomycin A1	LC Laboratories	Cat# B1080
NuPage 12% bis-tris gel 12 well	Novex	Cat# NP0342BOX
NuPage 12% bis-tris gel 15 well	Novex	Cat# NP0343BOX
NuPage 12% bis-tris gel 17 well	Novex	Cat# NP0349BOX
Novex sharp pre-stained protein standard	Novex	Cat# LC5800
MOPS SDS running buffer	Novex	Cat# NP0001
Transfer buffer	Novex	Cat# NP0006
Recombinant human CCL19	Peprotech	Cat# 300-29B
Recombinant human IL7	Peprotech	Cat# 200-07
Recombinant human IL2	Roche	Cat# 10799068001
Recombinant human TNF	RnD Systems	Cat# 210-TA
Birinapant	Selleck Chemicals	Cat# S7015
Embelin	Selleck Chemicals	Cat# S7025
GDC-0152	Selleck Chemicals	Cat# S7010
Vorinostat	Selleck Chemicals	Cat# S1047
z-VAD-FMK	Selleck Chemicals	Cat# S8102
2-sulfanylethan-1-ol	Sigma	Cat# M3148
12-O-Tetradecanoylphorbol-13-acetate	Sigma	Cat# P1585
Actinomycin D	Sigma	Cat# A9415
Bovine serum albumin (BSA)	Sigma	Cat# A9418
Chloroquine diphosphate salt	Sigma	Cat# C6628
Dimethyl sulphoxide	Sigma	Cat# D2650
EDTA	Sigma	Cat# E7889
Fetal bovine serum (15H095H2)	Sigma	Cat# F4135
Necrostatin-1	Sigma	Cat# N9037
OptiPrep	Sigma	Cat# D1556
Phytohemagglutinin PHA-P from *Phaseolus vulgaris*	Sigma	Cat# L8754
Polyoxyethylenesorbitan monolaurate	Sigma	Cat# P7949
Staurosporine solution from Streptomyces sp	Sigma	Cat# S6942
Sodium azide	Sigma	Cat# S2002
Triton-X 100	Sigma	Cat# X100

(*Continued on next page*)

Continued

REAGENT or RESOURCE	SOURCE	IDENTIFIER
Wortmannin	Sigma	Cat# W3144
Halt protease and phosphatase inhibitor cocktail	Thermo Scientific	Cat# 78440
Pierce lane marker reducing sample buffer	Thermo Scientific	Cat# 39000
Proteinase K	Thermo Scientific	Cat# AM2546
Critical Commercial Assays		
ssDNA apoptosis ELISA kit	Chemicon	Cat# APT225
PureLink genomic DNA mini kit	Invitrogen	Cat# K182001
TNF alpha Human ELISA Kit, High Sensitivity	Invitrogen	Cat# BMS223HS
Human CD4+ T cell isolation kit	Miltenyi Biotec	Cat# 130-096-533
Human memory CD4+ T cell isolation kit	Miltenyi Biotec	Cat# 130-091-893
α-human CD8 microbeads	Miltenyi Biotec	Cat# 130-045-201
α-human CD25 microbeads II	Miltenyi Biotec	Cat# 130-092-983
anti-biotin microbeads	Miltenyi Biotec	Cat# 130-090-485
α-human CD69 biotin	Miltenyi Biotec	Cat# 130-092-161
α-human HLA-DR microbeads	Miltenyi Biotec	Cat# 130-046-101
Dead cell apoptosis kit with annexin V Alexa Fluor 488 & propidium iodide (PI)	Molecular Probes	Cat# V13241
Alliance HIV p24 antigen ELISA kit	Perkin Elmer	Cat# NEK050B001KT
QIAamp viral RNA Mini	Qiagen	Cat# 52906
LightCycler FastStart DNA Master HybProbe	Roche	Cat# 12239272001
LightCycler 480 genotyping master	Roche	Cat# 04707524001
LightCycler 480 RNA master hydrolysis probes	Roche	Cat# 04991885001
Cell Proliferation Reagent WST-1	Roche	Cat# 11644807001
Pierce co-immunoprecipitation kit	Thermo Scientific	Cat# 26149
Experimental Models: Cell Lines		
NCTC clone 929 [L cell, L-929, derivative of Strain L]	ATCC	Cat# CCL-1, RRID: CVCL_0462
ACH-2	National Institute of Health – AIDS Reagent Program	Cat# 349-443, RRID:CVCL_0138
A3.01	National Institute of Health – AIDS Reagent Program	Cat# 166-382, RRID:CVCL_6244
HEK-293	National Institute of Health – AIDS Reagent Program	Cat# 103-306, RRID:CVCL_0045
TZM-bl	National Institute of Health – AIDS Reagent Program	Cat# 8129-442, RRID:CVCL_B478
Oligonucleotides		
See Table S1 for primers used		
See Table S1 for shRNA Lentiviral Transduction Particles used		
Software and Algorithms		
GraphPad Prism 7	GraphPad Software	RRID: SCR_002798; https://www.graphpad.com/
ImageJ 1.50b	NIH	RRID:SCR_003070; https://imagej.nih.gov/ij/
FlowJo v10	Tree Star	RRID: SCR_008520; https://www.flowjo.com/
BD CellQuest Pro	BD Biosciences	RRID:SCR_014489

CONTACT FOR REAGENT AND RESOURCE SHARING

Further information and requests for resources and reagents should be directed to and will be fulfilled by the Lead Contact, Stephen A. Spector (saspector@ucsd.edu).

EXPERIMENTAL MODEL AND SUBJECT DETAILS

Cell Culture

The following cell lines were obtained through the NIH AIDS Reagent Program, Division of AIDS: ACH-2 (human; sex: female) and A3.01 (human; sex: female) from Dr. Thomas Folks (Buttke and Folks, 1992; Clouse et al., 1989; Folks et al., 1989), HEK-293 (human; sex: female) from Dr. Andrew Rice (Graham et al., 1977), and TZM-bl (human; sex: female) from Dr. John C. Kappes, Dr. Xiaoyun Wu and Tranzyme Inc. (Wei et al., 2002). HEK-293 and TZM-bl cells were maintained in Dulbecco's modified Eagle's medium (DMEM) supplemented with 10% (vol/vol) heat-inactivated FBS, 0.1 g L^{-1} streptomycin, 10^5 U L^{-1} penicillin (all Gibco) in 5% CO_2 at 37°C. ACH-2 and A3.01 cells were maintained in RPMI 1640 supplemented with 10% (vol/vol) heat-inactivated FBS, 10 mM 2-(4-(2-hydroxyethyl)piperazin-1-yl)ethanesulfonic acid (HEPES), 0.1 g L^{-1} streptomycin, 10^5 U L^{-1} penicillin (all Gibco) in 5% CO_2 at 37°C. NCTC clone 929 cells (murine; sex: male) were obtained from ATCC and were cultured in RPMI 1640 supplemented with 10% (vol/vol) heat-inactivated FBS in 5% CO_2 at 37°C.

Primary Human Cells

Whole blood (360 mL) was drawn from HIV-seronegative healthy volunteers, ages between 18 and 65 years, at UC San Diego Health Sciences. In accordance with the Human Research Protections Program of the University of California, San Diego, all samples were de-identified and donors remained anonymous. Thus, the authors did not obtain personal identifying information and cannot report on their sex, gender identity, or age. Samples were assigned to experimental protocols through simple random sampling. PBMC were isolated by density gradient centrifugation over Ficoll-Paque Plus (GE Healthcare). PHA stimulated PBMC (PHA-PBMC) were prepared by incubating 2×10^6 PBMC mL^{-1} in expansion media (RPMI 1640 supplemented with 20% [vol/vol] heat-inactivated FBS, 2 mM L-glutamine, 0.1 g L^{-1} streptomycin, 10^5 U L^{-1} penicillin [all Gibco], and 10000 U L^{-1} IL2 [Roche]) supplemented with 1 mg mL^{-1} PHA-P for 48 hr in 5% CO_2 at 37°C. Resting CD4+ T cells were purified from unstimulated PBMC by negative selection using the Miltenyi Biotec human CD4+ T Cell Isolation Kit supplemented with a biotin-conjugated anti-HLA-DR antibody (clone AC122; Miltenyi Biotec). Whole blood (200 mL) was drawn from HIV-infected volunteers aged between 18 and 65 years at the UCSD Mother-Child-Adolescent HIV Program. Individuals were selected on the basis of sustained suppression of plasma viral load (< 20 copies mL^{-1} for > 6 months) during ART and CD4+ T cell counts of > 400 cells μL^{-1}. In accordance with the Human Research Protections Program of the University of California, San Diego, all samples were de-identified and donors remained anonymous, thus the authors did not obtain personal identifying information and cannot report on their sex, gender identity, or age. Sample size was determined using a 2-sample 2-sided equality test with power $(1-\beta) = 0.8$, $\alpha = 0.05$ and preliminary data where the minimum difference in outcome was at least 70%.

Ethical Statement

Venous blood was drawn from human subjects using protocols that were reviewed and approved by the Human Research Protections Program of the University of California, San Diego in accordance with the requirements of the Code of Federal Regulations on the Protection of Human Subjects (45 CFR 46 and 21 CFR 50 and 56) and were fully compliant with the principles expressed in the Declaration of Helsinki. All volunteers gave written informed consent prior to their participation.

Virus

The infectious molecular clone of HIV strain NL4-3 (pNL4-3) was obtained through the NIH AIDS Reagent Program from Dr Malcolm Martin (Adachi et al., 1986). For virus preparation, HEK293T cells were transfected with proviral DNA using the calcium phosphate method (He et al., 1995). Virus was harvested at 48 and 72 hr post-transfection then filtered through a 0.22 μm polyethersulfone filter (Millipore). Virus-containing supernatants were harvested 2 days later, and cellular debris was removed by centrifugation (5 min, 300 × *g*) followed by filtration through a 0.22 μm polyethersulfone filter (Millipore). Virus was then expanded using 2×10^6 PHA-PBMC mL^{-1} in expansion media for 4 weeks in 5% CO_2 at 37°C. Fresh expansion media was added twice per week, and fresh PHA-PBMC were added once per week. Viral stocks were concentrated as previously described (Campbell and Spector, 2008). Viral concentrates were subjected to a 6 to 18% iodixanol velocity gradient in 1.2% increments using OptiPrep (60% [w/v] iodixanol; Sigma) diluted in DPBS as previously described (Dettenhofer and Yu, 1999). Briefly, supernatants were laid over the gradient and centrifuged for 1.5 hr at 37,500 rpm (250,000 × g at r_{max}) in an SW41 Ti rotor using an L8-70M ultracentrifuge (both Beckman Coulter). Fourteen gradient fractions were collected and analyzed for total protein and HIV p24 content by SDS-PAGE and western blot analysis. HIV infectivity was calculated as the 50% tissue culture infectious doses ($TCID_{50}$) using PHA-PBMC and the Alliance HIV p24 antigen ELISA (Perkin Elmer) as described previously (Japour et al., 1993) and multiplicity of infection confirmed using TZM-bl cells.

METHOD DETAILS

Establishment of Resting, HIV Infected CD4+ T Cells

This primary cell model is adapted from two previously established methods (Marini et al., 2008; Saleh et al., 2011) and recapitulates the events of *in vivo* infection: namely infection, clonal expansion, and subsequent contraction. The first step relies upon the findings that *in vitro* latent infection can be established in resting CD4+ T cells through C-C motif chemokine ligand (CCL) 19 pretreatment

(Saleh et al., 2011). Purified resting HIV uninfected CD4+ T cells were incubated for 48 hr in 5% CO_2 at 37°C in growth media (RPMI 1640 supplemented with 10% [vol/vol] heat-inactivated FBS, 50 μM 2-sulfanylethan-1-ol [both Sigma], 100 μM nonessential amino acids, 1 mM sodium pyruvate, 0.1 g L^{-1} streptomycin, 10^5 U L^{-1} penicillin [all Gibco]) supplemented with 29 nM CCL19 (R&D Systems) before infection with 0.4 MOI (multiplicity of infection) HIV_{NL4-3} for 3 h in 5% CO_2 at 37°C as previously described by the Lewin laboratory (Saleh et al., 2011). The second step is adapted from the Romerio laboratory (Marini et al., 2008). Cells were washed three times to remove cell-free virus, plated at 5 × 10^5 cells mL^{-1} in fresh growth media supplemented with 250 μg L^{-1} staphylococcal enterotoxin B (Sigma) and 25000 U L^{-1} IL2 (Roche), and cultured for 3 days in 5% CO_2 at 37°C. Cells were then washed and resuspended at 5 × 10^5 cells mL^{-1} in fresh growth media supplemented with 25000 U L^{-1} IL2 and cultured for 12 days in 5% CO_2 at 37°C. Every 2-3 days, fresh IL2-containing media was added to bring the cell concentration back to 5 × 10^5 cells L^{-1} and supernatant HIV p24 release measured using the Alliance HIV p24 antigen ELISA (Figures S1A–S1C). Memory CD4+ T cells were enriched by negative selection from 12 day cultures of HIV-infected and uninfected CD4+ T cells using a memory CD4+ T cell isolation kit (Miltenyi Biotec) (Figures S1D). Highly enriched cells were then cultured in basal media (RPMI 1640 supplemented with 10% (vol/vol) heat-inactivated FBS, 0.1 g L^{-1} streptomycin, 10^5 U L^{-1} penicillin), supplemented with 1 μg L^{-1} IL7 (R&D Systems) for up to 30 days in 5% CO_2 at 37°C to return to a quiescent status. Cell death was estimated using the lactate dehydrogenase (LDH) Cytotoxicity Detection Kit^{PLUS} (Roche), trypan blue exclusion assay, the single stranded DNA ELISA (Millipore) (Campbell et al., 2011), and by flow cytometry. After 20 d, the HIV infected, resting central memory CD4+ T cells (HIV-T_{CM}) lack both cell surface activation and cell cycle markers, do not synthesize DNA, do not proliferate, and contain an average of 1 copy per cell of integrated HIV DNA (Figures S1E–S1H). The intracellular HIV p24 detected within infected cells likely represents residual HIV proteins expressed during the expansion phase that are undergoing degradation during the contraction and resting phase in the absence of *de novo* production. Importantly, HIV can be reactivated from these cells using αCD3/αCD28-conjugated beads (1:1 bead:cell ratio) for 72 hr, 10 mg L^{-1} phytohemagglutinin (PHA-M) for 48 hr, 1 μM vorinostat (SAHA) for 24 hr, or 100 μg L^{-1} IL7 for 120 hr (Figure S1I). Cells were incubated in basal media in 5% CO_2 at 37°C for 24 hr before SM treatment. All subsequent experiments were performed in basal media in 5% CO_2 at 37°C.

Latent HIV Limiting Dilution Co-culture Assay

HIV-infected individuals followed at the UCSD Mother-Child-Adolescent HIV Program were selected on the basis of sustained suppression of plasma viral load (<20 copies mL^{-1} for >6 months) during ART and CD4+ T cell counts of >400 cells μL^{-1}. Resting CD4+ T cells were isolated by depletion from HIV-infected donor PBMC using a CD4+ T cell isolation kit (Miltenyi Biotec), followed by further depletion using CD69-biotin, CD25, HLA-DR and biotin microbeads (all Miltenyi Biotec). Cells were then treated with SM at 5 × 10^5 cells mL^{-1} in RPMI 1640 supplemented with 10% (vol/vol) heat-inactivated FBS, 0.1 g L^{-1} streptomycin, and 10^5 U L^{-1} penicillin for 24 hr in 5% CO_2 at 37°C. Supernatants were collected and stored at -80°C for future RT-qPCR and HIV p24 ELISA analysis. CD4+ T cells were then serially diluted and subjected to a limiting dilution quantitative virus outgrowth assay (QVOA) to demonstrate the presence and persistence of latent HIV in patient cells as previously described (Laird et al., 2016). Donors were excluded from the study if we were unable to reactivate virus under any treatment condition or if we were unable to obtain sufficient cell numbers to perform the assay.

Flow Cytometry

For analysis of CD4+ T cell phenotypes, 1 × 10^6 cells were washed with Dulbecco's phosphate buffered saline supplemented with 10 g L^{-1} bovine serum albumin and 15.4 mM NaN_3 (both Sigma; FACS buffer), and then resuspended in 100 μL of the same buffer containing fluorescently labeled monoclonal antibodies against CD3 (SK7), CD4 (L200), CD25 (M-A251), CD45RO (UCHL1), CD45RA (HI100), CD62L (DREG-56), CD69 (FN50), CCR7 (150503), or HLA-DR (G46-6) (all from BD Biosciences) for 30 min on ice and in the dark. Cells were then washed with FACS buffer, fixed and permeabilized using BD Cytofix/Cytoperm (BD Biosciences) for 30 min on ice and in the dark. Cells were washed in BD Perm/Wash Buffer (BD Biosciences) and resuspended in the same buffer supplemented with fluorescently labeled monoclonal antibodies against MKI67 (B56; BD Biosciences), washed and resuspended in FACS buffer.

To differentiate between early apoptosis and late apoptosis/necrosis, cells were harvested over 24 hr post-treatment, stained with Alexa Fluor 488-tagged ANXA5 and propidium iodide (both Molecular Probes). For mixed cell populations, mock-infected cells were tagged with peridinin chlorophyll-cyanine 5.5-tagged anti-CD4 antibodies and HIV-infected cells were tagged with Alexa Fluor 647-tagged anti-CD4 antibodies (both BD Biosciences) prior to mixing. Cell death was estimated using Alexa Fluor 488-tagged ANXA5 and PI staining and flow cytometry in a blinded assay. Blinded analysis was performed using a BD FACSCalibur flow cytometer and analyzed using Cell Quest Pro (both BD Biosciences).

Lactate Dehydrogenase Activity

To assess the extent of necrotic cell death, lactate dehydrogenase (LDH) activity of supernatants was measured using a mixture of diaphorase/NAD+ and 3-(4-iodophenyl)-2-(4-nitrophenyl)-5-phenyl-2H-tetrazol-3-ium chloride/sodium 2-hydroxypropanoate according to the manufacturer's protocol (Roche).

Chemicals

Birinapant, GDC-0152, embelin, and vorinostat (suberoylanilide hydroxamic acid) were purchased from Selleck Chemicals. Concentrations of drugs used were based upon previously published whole blood C_{max} and C_{min} data for each drug (Amaravadi et al., 2015; Flygare et al., 2012; Zutshi et al., 1990) and were prepared in dimethyl sulfoxide. Corresponding volumes of DMSO (5μL DMSO

per mL) were used for the vehicle in each experiment. Staurosporine was purchased from Sigma and was used at 1 μM. For inhibitor experiments, 20 μM z-VAD-FMK, 200 nM wortmannin, 10 μM chloroquine, 10 nM bafilomycin A_1, or 10 μM necrostatin-1 (all Sigma) were added for 1 hr prior to, and for the duration of the stimulation. The human TNF neutralizing antibody (D1B4) was purchased from Cell Signaling, and was added 2 hr prior to SM treatment at 1 μg mL^{-1}.

Anti-TNF Neutralization Assay

Neutralizing activities of D1B4 against TNF was measured essentially as previously described (Matthews and Neale, 1987). Briefly, NCTC clone 929 cells (ATCC) were seeded in triplicate at 3 × 10^5 cells $well^{-1}$ in a 96 well plate and cultured in RPMI 1640 supplemented with 10% (vol/vol) heat-inactivated FBS for 16 hr in 5% CO_2 at 37°C. Fresh RPMI 1640 (without phenol red) supplemented with 10% (vol/vol) heat-inactivated FBS, 1 μg mL^{-1} actinomycin D (Sigma), 1 ng mL^{-1} TNF (RnD Systems), and 0.1-100 ng ml^{-1} antibody D1B4 was prepared and added to cells for 19 hr in 5% CO_2 at 37°C. WST-1 was then added at a 1:10 final dilution and incubated in 5% CO_2 at 37°C for 1 hr. The color change in each well was recorded on an ELX800 (BioTek) at 450nm.

shRNA Transduction

Lentiviral transduction with MISSION lentiviral particles containing short hairpin RNA (shRNA) targeting *ATG2A* (SHCLNV-NM_015104/TRCN0000168420), *ATG2B* (SHCLNV-NM_029654/TRCN0000150114), *ATG5* (SHCLNV-NM_004849/TRCN0000151963), *ATG7* (SHCLNV-NM_006395/TRCN0000007584), *RUBCN* (SHCLNV-NM_001145642/TRCN0000235638), *SQSTM1* (SHCLNV-NM_003900/TRCN0000007237), *ULK1* (SHCLNV-NM_003565/TRCN0000000835), or scrambled non-target negative control (SHC002V) was performed according to the manufacturer's protocol (Sigma). SHC002V was used as non-targeting negative control as it activates the RNA-induced silencing complex and the RNAi pathway, but does not target any human gene allowing the examination of the effects of shRNA transduction and RNAi activation on gene expression. CD4+ T cells were transduced with non-specific scrambled shRNA (shNS) or target shRNA and selected using 3 mg L^{-1} puromycin (Gibco). For simultaneous silencing of *ATG2A* and *ATG2B*, cells were selected with 3 mg L^{-1} puromycin and 200 mg L^{-1} G418 (Gibco). Five days later, cells were analyzed for target gene silencing and used in experiments.

Western Blotting

ATG2A (#15011), ATG5 (#2630), ATG7 (#2631), BECN1 (#3738), BIRC2 (D5G9), CASP8 (1C12), FADD (#2782), FAS (C18C12), FASLG (#4273), HSP90 (C45G5); LAMP1 (C54H11), MLKL (D2I6N), PARP1 (46D11), RIPK1 (D94C12), RIPK3 (D4G2A), ULK1 (D9D7), and XIAP (3B6) antibodies were obtained from Cell Signaling. SQSTM1 (#ab56416), tubulin beta class I (TUBB; #ab21058), and STX17 (#ab116113) antibodies were purchased from abcam. β-actin (ACTB; AC-74) and ATG2B (#HPA019665) were purchased from Sigma. MAP1LC3B (#NB100-2220) was purchased from Novus Biologicals. Cell lysates were prepared using 20 mM HEPES (Gibco), 150 mM NaCl (Fisher), 1 mM 2,2',2'',2'''-(ethane-1,2-diyldinitrilo)tetraacetic acid supplemented (Sigma) with 1% (vol/vol) 4-(1,1,3,3-tetramethylbutyl)phenyl-polyethylene glycol (Triton X-100; Sigma) and 1% (vol/vol) Halt protease and phosphatase inhibitor cocktail (Thermo Scientific). For co-immunoprecipitation, 50 μg anti-CASP8 or anti-RIPK1 were immobilized in a coupling gel then 50 μg cell lysates were incubated with the antibody-immobilized coupling gel using the Thermo Scientific Pierce Co-Immunoprecipitation Kit. Cell lysates were resolved using 2-[bis(2-hydroxyethyl)amino]-2-(hydroxymethyl)propane-1,3-diol buffered 12% polyacrylamide gel (Novex) and transferred to 0.2 μm polyvinylidene difluoride membranes (Thermo Scientific), followed by detection with primary antibodies followed by alkaline phosphatase tagged secondary antibodies (Invitrogen) and 0.25 mM disodium 2-chloro-5-(4-methoxyspiro[1,2-dioxetane-3,2′-(5-chlorotricyclo[3.3.1.1^{3,7}]decan])-4-yl]-1-phenyl phosphate supplemented with 5% (vol/vol) Nitro-Block II (both Applied Biosystems). Relative densities of the target bands were compared to the references ACTB, TUBB, CASP8, or RIPK1 bands and were calculated using ImageJ (NIH). Each data point was normalized to the vehicle then log_2 transformed.

Subcellular Fractionation and Proteinase K Treatment

Subcellular fractionation was performed as previously described (Velikkakath et al., 2012). Briefly, vehicle treated HIV-T_{CM} or HIV-T_{CM} simultaneously exposed to 100 nM birinapant and 200 nM bafilomycin A_1 for 2 hr were homogenized in 10 mM HEPES-KOH, pH 7.4, supplemented with 0.22 M D-mannitol, 0.07 M sucrose, and protease inhibitors with 10 strokes of a 27 gauge needle. The post-nuclear supernatant (PNS) was centrifuged at 300 × *g* for 5 min to remove cell debris. The PNS was spun at 7700 × *g* for 5 min to separate the low speed pellet (LSP). The supernatant from this step was then centrifuged at 100,000 × *g* for 30 min to generate a high speed pellet (HSP) and a high speed supernatant (HSS). LSP and HSP were resuspended in 10 mM HEPES-KOH, pH 7.4, supplemented with 0.22 M D-mannitol, 0.07 M sucrose, and protease inhibitors and washed. To examine proteinase K sensitivity, each fraction was treated with 100 μg mL^{-1} proteinase K on ice for 20 min with or without 0.5% (vol/vol) Triton X-100. Samples were precipitated with 10% trichloroacetic acid, washed once with ice-cold propan-2-one, resuspended in Thermo Scientific Pierce lane marker reducing sample buffer, boiled, and resolved using 2-[bis(2-hydroxyethyl)amino]-2-(hydroxymethyl)propane-1,3-diol buffered 12% polyacrylamide gel (Novex).

Quantitative Real-Time PCR

HIV integrated DNA was quantified using a previously described nested Alu-LTR quantitative real-time PCR (qPCR) blinded assay with some minor modifications to account for the different machines used (Lewin et al., 2008). Briefly, high-molecular-weight DNA was extracted from 2 × 10^6 cells using the PureLink genomic DNA mini kit (Invitrogen) as recommended by the manufacturer and normalized using a NanoDrop Lite (Thermo Scientific) to 50 μg mL^{-1}, then stored at-20°C until used. For the first round Alu-LTR PCR reaction, 5 μL of DNA was added to the first-round PCR mix with a final concentration of 1 × PCR buffer (Invitrogen), 1.25 U of AmpliTaq Gold DNA polymerase, 2.5 mM of $MgCl_2$, 1 mM of deoxynucleoside triphosphate, and 0.3 μM of each primer (HIV LTR forward primer MH535 [5'-AACTAGGGAACCCACTGCTTAAG-3'] and genomic Alu reverse primer SB704 [5'-TGCTGGGATTA CAGGCGTGAG-3']) as previously described (Butler et al., 2001; Lewin et al., 2008). The first-round Alu-LTR PCR was performed in a GeneAmp PCR System 9700 (Applied Biosystems), with the following cycling conditions: 95°C for 10 min, then 18 cycles with the following parameters: 15 s at 95°C, 60 s at 60°C, then 100 s at 72°C. 5 μL of the first-round product was then added to a second-round LTR-LTR qPCR mix with a final concentration of 1 × LightCycler 480 Genotyping Master (Roche Applied Science), 0.5 μM of each primer (HIV LTR forward primer SL75 [5'-GGAACCCACTGCTTAAGCCTC-3'] and HIV LTR reverse primer SL76 [5'- GTCTGAGGGATCTCTAGTTACC-3']), and 0.2 μM HIV-LTR beacon SL72 (5'-(FAM)-CGGTCGAGTGCTTCAAG TAGTGTGTGCCCGTCCGACCG-(TAMRA)-3' (Lewin et al., 2008). The second-round LTR-LTR qPCR was performed in a Roche Light Cycler 480 II (Roche Applied Science), with the following cycling conditions: sample was heated to 95°C followed by 45 cycles with the following parameters: 15 s at 95°C, 45 s at 65°C, and 45 s at 72°C, with a temperature transition rate of 4.4°C s^{-1} for all steps apart from the annealing step (2.2°C s^{-1}). A single fluorescence acquisition was performed after each elongation step. A standard that contained integrated HIV DNA at random locations was performed as previously described (Lewin et al., 2008). To normalize for cell equivalents of input DNA, we performed a separate qPCR with primers and probes to detect the number of *hemoglobin subunit beta* (*HBB*) copies as previously described (MacKenzie et al., 2003; Townson et al., 2002) using the LightCycler FastStart DNA Master HybProbe kit with the following cycling conditions: sample was heated to 95°C followed by 40 cycles with the following parameters: 15 s at 95°C, 30 s at 60°C, and 60 s at 72°C, with a temperature transition rate of 4.4°C s^{-1} for all steps apart from the annealing step (2.2°C s^{-1}). A single fluorescence acquisition was performed after each elongation step. Results were calculated using the Pfaffl method (Pfaffl, 2001).

Total viral RNA was extracted directly from cell culture supernatants using the QIAamp viral RNA Mini (Qiagen). Measurement of HIV transcripts was performed as previously described (Gorantla et al., 2010). Briefly, HIV transcripts were measured by reverse transcription qPCR (RT-qPCR) with primer pairs that detect single-spliced viral transcripts (5′-ACATCAAGCCATGCAAAT-3′, and 5′-ATCTGGCCTGGTGCAATAGG-3′) and probe (5'-(5HEX)-CATCAATGA-(ZEN)-GGAAGCTGCAGAATGGGATAG-(3IABKFQ)-3') using a Roche Light Cycler 480 II and the LightCycler 480 RNA master hydrolysis probes kit (Roche Applied Science) (Vicenzi et al., 2002). The reaction mixtures were initially incubated at 63°C for 3 min to reverse transcribe the RNA. The sample was then heated to 95°C for 30 s to denature the cDNA. Amplification was performed for 45 cycles, with the following cycle parameters: 10 s of denaturation at 95°C, 30 s of primer annealing at 60°C, and 1 s of fragment elongation at 72°C, with a temperature transition rate of 4.4°C s^{-1} for all steps apart from the annealing step (2.2°C s^{-1}). A single fluorescence acquisition was performed after each elongation step. Results were calculated using the Pfaffl method (Pfaffl, 2001). Researchers were blinded as to the provenance and treatment of the samples.

Statistics

Samples were assigned to experimental groups through simple random sampling. Sample size was determined using a 2-sample 2-sided equality test with power (1-β) = 0.8, α = 0.05 and preliminary data where the minimum difference in outcome was at least 70%. Sample sizes are denoted in figure legends and refer to the number of donors (independent biological replicates [*n*]). Data are represented as dot blots with means and error bars for independent biological replicates, and as the mean with no error bars for technical replicates (cell line data). Data were assessed for symmetry, or skewness, using Pearson's skewness coefficient. Fold change data were log_2 transformed to convert the ratio to a difference that better approximates the normal distribution on a log scale. When expression in the reference sample (*Rij*) is low, or when *Rij* = 0, we get extreme estimates or missing values for the log_2 ratio. In these cases, we used the proportion of protein expression in the test sample. The proportion takes the amount of protein in the test sample and compares it to the total amount of expressed or bound protein represented by the sum of the test and reference samples (Bergemann and Wilson, 2011). Comparisons between groups were performed using the paired, two-tailed, Student's *t* test. *P value*s were determined on the basis of biological replicates (with technical replicates averaged within each biological replicate). In all experiments, differences were considered significant when *P* was less than 0.05. *P < 0.05.